Regional climate model simulations for Europe at 6 and 0.2 k BP

sensitivity to changes in anthropogenic deforestation

Strandberg, G.; Kjellstrom, E.; Poska, A.; Wagner, Stefan; Gaillard, M. -J.; Trondman, A. -K.; Mauri, A.; Davis, B. A. S.; Kaplan, J. O.; Birks, H. J. B.; Bjune, A. E.; Fyfe, R.; Giesecke, T.; Kalnina, L.; Kangur, M.; van der Knaap, W. O.; Kokfelt, Ulla; Kunes, P.; Latalowa, M.; Marquer, L.; Mazier, F.; Nielsen, A. B.; Smith, B.; Seppa, H.; Sugita, S.

Published in:
Climate of the Past

DOI:
10.5194/cp-10-661-2014

Publication date:
2014

Document version
Publisher's PDF, also known as Version of record

Clim. Past, 10, 661–680, 2014
www.clim-past.net/10/661/2014/
doi:10.5194/cp-10-661-2014

Climate of the Past
Open Access

Regional climate model simulations for Europe at 6 and 0.2 k BP: sensitivity to changes in anthropogenic deforestation

G. Strandberg[1,2], E. Kjellström[1,2], A. Poska[3,5], S. Wagner[4], M.-J. Gaillard[5], A.-K. Trondman[5], A. Mauri[6], B. A. S. Davis[6], J. O. Kaplan[6], H. J. B. Birks[7,8,9,22,23], A. E. Bjune[10], R. Fyfe[11], T. Giesecke[12], L. Kalnina[13], M. Kangur[14], W. O. van der Knaap[15], U. Kokfelt[16,3,5], P. Kuneš[17], M. Latałowa[18], L. Marquer[5], F. Mazier[19,3], A. B. Nielsen[20,5], B. Smith[3], H. Seppä[21], and S. Sugita[14]

[1]Swedish Meteorological and Hydrological Institute, Norrköping, Sweden
[2]Department of Meteorology, Stockholm University, Stockholm, Sweden
[3]Department of Earth and Ecosystem Science, Lund University, Lund, Sweden
[4]Helmholtz-Zentrum Geesthacht, Geesthacht, Germany
[5]Department of Biology and Environmental Science, Linnaeus University, Kalmar, Sweden
[6]Institute for Environmental Sciences, University of Geneva, Geneva, Switzerland
[7]Department of Biology and Bjerknes Centre for Climate Research, University of Bergen, Bergen, Norway
[8]Environmental Change Research Centre, University College London, London, UK
[9]School of Geography and the Environment, University of Oxford, Oxford, UK
[10]Uni Climate, Uni Research AS and Bjerknes Centre for Climate Research, Bergen, Norway
[11]School of Geography, Earth and Environmental Sciences, University of Plymouth, Plymouth, UK
[12]Department of Palynology and Climate Dynamics, Albrecht-von-Haller Institute for Plant Sciences, University of Göttingen, Göttingen, Germany
[13]Faculty of Geography and Earth Sciences, University of Latvia, Riga, Latvia
[14]Institute of Ecology, Tallin University, Tallin, Estonia
[15]Institute of Plant Sciences and Oeschger Centre for Climate Change Research, University of Bern, Bern, Switzerland
[16]Center for Permafrost, Department of Geosciences and Natural Resource Management, University of Copenhagen, Copenhagen, Denmark
[17]Department of Botany, Faculty of Science, Charles University in Prague, Prague, Czech Republic
[18]Laboratory of Palaeoecology and Archaeobotany, Department of Plant Ecology, University of Gdańsk, Gdańsk, Poland
[19]GEODE, UMR 5602, University of Toulouse, Toulouse, France
[20]Department of Geology, Lund University, Lund, Sweden
[21]Department of Geosciences and Geography, University of Helsinki, Helsinki, Finland
[22]Environmental Change Research Centre, University College London, London, UK
[23]School of Geography and the Environment, University of Oxford, Oxford, UK

Correspondence to: G. Strandberg (gustav.strandberg@smhi.se)

Received: 30 September 2013 – Published in Clim. Past Discuss.: 18 October 2013
Revised: 27 January 2014 – Accepted: 17 February 2014 – Published: 28 March 2014

Abstract. This study aims to evaluate the direct effects of anthropogenic deforestation on simulated climate at two contrasting periods in the Holocene, ∼ 6 and ∼ 0.2 k BP in Europe. We apply We apply the Rossby Centre regional climate model RCA3, a regional climate model with 50 km spatial resolution, for both time periods, considering three alternative descriptions of the past vegetation: (i) potential natural vegetation (V) simulated by the dynamic vegetation model LPJ-GUESS, (ii) potential vegetation with anthropogenic land use (deforestation) from the HYDE3.1 (History Database of the Global Environment) scenario (V + H3.1), and (iii) potential vegetation with anthropogenic land use

Published by Copernicus Publications on behalf of the European Geosciences Union.

from the KK10 scenario (V + KK10). The climate model results show that the simulated effects of deforestation depend on both local/regional climate and vegetation characteristics. At ∼ 6 k BP the extent of simulated deforestation in Europe is generally small, but there are areas where deforestation is large enough to produce significant differences in summer temperatures of 0.5–1 °C. At ∼ 0.2 k BP, extensive deforestation, particularly according to the KK10 model, leads to significant temperature differences in large parts of Europe in both winter and summer. In winter, deforestation leads to lower temperatures because of the differences in albedo between forested and unforested areas, particularly in the snow-covered regions. In summer, deforestation leads to higher temperatures in central and eastern Europe because evapotranspiration from unforested areas is lower than from forests. Summer evaporation is already limited in the southernmost parts of Europe under potential vegetation conditions and, therefore, cannot become much lower. Accordingly, the albedo effect dominates in southern Europe also in summer, which implies that deforestation causes a decrease in temperatures. Differences in summer temperature due to deforestation range from −1 °C in south-western Europe to +1 °C in eastern Europe. The choice of anthropogenic land-cover scenario has a significant influence on the simulated climate, but uncertainties in palaeoclimate proxy data for the two time periods do not allow for a definitive discrimination among climate model results.

1 Introduction

Humans potentially had an influence on the climate system through deforestation and early agriculture already long before we started to emit CO_2 from fossil fuel combustion (Ruddiman, 2003). Deforestation affects the climate at many scales, from microclimate to global climate (e.g. Bala et al., 2007). The effect on the global climate is conveyed by the increased amounts of CO_2 in the atmosphere from deforestation, and by the regional and local changes of land-surface properties (e.g. Forster et al., 2007). Such changes have a direct effect on the regional climate, including changes in albedo and energy fluxes between the land surface and the atmosphere (e.g. Pielke et al., 2011). Since forests generally have a lower reflectivity than unforested areas, the albedo effect from deforestation would lead to lower regional temperature. Reduced vegetation cover also means reduced evapotranspiration that leads to higher air temperature, but the amplitude of the evapotranspiration changes depend on local conditions, such as soil moisture availability (Ban-Weiss et al., 2011; de Noblet-Ducoudré et al., 2012). The effects of increased atmospheric CO_2 resulting from changing vegetation and land use over the last 8000 yr have been previously discussed (e.g. Ruddiman, 2003; Pongratz et al., 2009a). The direct effects of past vegetation change have mostly been studied on a global scale (e.g. Brovkin et al., 2006; Pitman et al., 2009; Pongratz et al., 2009b, 2010; de Noblet-Ducoudré et al., 2012; Christidis et al., 2013).

Global climate models (GCMs) are run on coarse spatial resolutions; therefore, they can only reproduce large-scale climate features. Regional climate models (RCMs) preserve the large-scale climate features, but the higher spatial resolution in RCMs provides a better representation of the land–sea distribution and topography, which in turn allows a more detailed description of the regional climate (Rummukainen, 2010). This also applies to vegetation modelling. Only a detailed description of vegetation can account for biogeophysical effects on climate at the regional scale (Wramneby et al., 2010). Since we expect vegetation change to affect climate at the local/regional spatial scale, a high spatial resolution in the climate model is critical when evaluating model results by comparison with observations and/or proxies that represent local to regional environment conditions. To date there are no previous RCM-based studies of the feedback on climate from historical changes in land use/anthropogenic land cover.

The present study investigates the direct effect on climate from human-induced vegetation changes in Europe at the regional spatial scale. We do not study the indirect effects from changing atmospheric CO_2 concentration. This study is part of the LANDCLIM (LAND cover–CLIMate interactions in NW Europe during the Holocene) project that aims to assess the possible effects on the climate of two historical processes (compared with a baseline of present-day land cover): (i) climate-driven changes in vegetation and (ii) human-induced changes in land cover (Gaillard et al., 2010). Specifically, this study asks (i) whether historical land use influences the regional climate, (ii) how much the RCM-simulated climate differs depending on the scenario of past anthropogenic land cover used, (iii) which processes are important for climate–vegetation interaction, and (iv) to what extent palaeoclimate proxy data are effective at evaluating RCM-based simulation results.

We focus on two contrasting time periods in terms of climate and anthropogenic land cover change: the Mid-Holocene warm period (∼ 6 k BP) and the Little Ice Age (∼ 0.2 k BP = ∼ AD 1750). The Mid-Holocene was characterised by a relatively warm climate and low human impact on vegetation/land cover, while the Little Ice Age was cool and anthropogenic land use was extensive. The 6 k time-window has the advantage of being widely used in model-data comparison studies of global climate models (e.g. Harrison et al., 1998; Masson et al., 1999; Kohfeld and Harrison, 2000; see the Palaeoclimate Modelling Intercomparison Project (PMIP) activities: http://pmip.lsce.ipsl.fr/), which allows us to set our results in a wider perspective. We use a dynamic vegetation model, LPJ-GUESS (Smith et al., 2001), to simulate past climate-driven potential natural vegetation and two alternative scenarios of anthropogenic land-cover change (ALCC): HYDE3.1 (History Database of the Global

Table 1. Summary of forcing conditions in the RCA3 simulations; see text for details. The amount of greenhouse gases and irradiance varies from year to year, and the table shows average values.

Name	Period	Vegetation	Land use	CO_2 (ppm)	CH_4 (ppb)	N_2O (ppb)	Total solar irradiance ($W\,m^{-2}$)
6 kV 6kV + H3.1 6kV + KK10	6 k BP	Potential 6 k	None HYDE3.1 KK10	265	572	260	1364
0.2 kV 0.2kV + H3.1 0.2kV + KK10	0.2 k BP	Potential 0.2 k	None HYDE3.1 KK10	277	710	277	1363

Environment; Klein Goldewijk et al., 2011) and KK10 (Kaplan et al., 2009). These scenarios of past human-induced vegetation are widely used in climate modelling of the past, but they exhibit large differences for key periods of the Holocene (Gaillard et al., 2010; Boyle et al., 2011). These discrepancies are due to differences in the modelling approach. While previous studies demonstrated the large influence of the choice of ALCC scenario on modelled changes in terrestrial carbon storage over the Holocene (Kaplan et al., 2009), little work has been done to assess the importance of the ALCC scenario used with respect to the biogeophysical feedback to climate. We therefore use both HYDE and KK10 in our model simulations of regional climate.

In order to evaluate the RCM-simulated results, we use climate proxy records based on (i) the LANDCLIM database of point data, i.e. representing either local or regional climate conditions based on non-pollen proxies (e.g. tree-ring data, chironomid records from lake sediments, stalagmite $\delta^{18}O$ records, etc.; Nielsen et al., 2014) to avoid any circular reasoning (where the same vegetation would be used both to force and evaluate the model simulations), and (ii) an attempt at spatially explicit descriptions of past climate characteristics based on pollen data (Mauri et al., 2013).

2 Material and methods

2.1 The models

The main tool used in this study to produce high spatial resolution climate simulations is the Rossby Centre regional climate model RCA3 (Samuelsson et al., 2011). Here, we describe RCA3 and the models that provide the boundary conditions for the RCA3 runs. These models include the global climate model ECHO-G (Legutke and Voss, 1999), the dynamic vegetation model (DVM) LPJ-GUESS (Smith et al., 2001), and the ALCC scenarios HYDE3.1 and KK10.

For each time period RCA3 uses lateral boundary conditions, sea-surface temperature and sea-ice conditions from ECHO-G and in the first run modern-day vegetation (Samuelsson et al., 2011). The simulated climate is then used to drive the vegetation model LPJ-GUESS to simulate potential vegetation. For each time period, three 50 yr long RCA3 simulations are then performed with three alternative land-cover/vegetation descriptions: (i) potential vegetation without human impact (V), (ii) V with the addition of the HYDE3.1 estimate of anthropogenic deforestation (V + H3.1), and (iii) V with the addition of the KK10 estimate of anthropogenic deforestation (V + KK10). The iterative modelling approach of RCM and DVM, RCA3 → LPJ-GUESS → RCA3, has been shown to be a reasonable approach where both simulated climate and vegetation are in general agreement with available reconstructions, which are few and uncertain (Kjellström et al., 2010; Strandberg et al., 2011). The simulations are summarised in Table 1. If not stated otherwise, "model simulation" stands for a simulation with RCA3 forced with data from the other models described below.

2.1.1 The general circulation model ECHO-G

ECHO-G has been used and evaluated earlier in palaeoclimatic studies (Zorita et al., 2005; Kaspar et al., 2007) and has provided climate simulations in regional studies (e.g. Gómez-Navarro et al., 2011, 2012; Schimanke et al., 2012). Here, we use results from the transient Oetzi2 run covering the period 7000 BP to present (Wagner et al., 2007). In Oetzi2, ECHO-G is run with a horizontal resolution of T30 (approximately $3.75° \times 3.75°$) and 19 levels in the atmosphere, and a spatial resolution of approximately $2.8° \times 2.8°$ and 20 levels in the oceans. The simulation was initialised at the end of a 500 yr spin-down control (quasi-equilibrium) run with constant forcing (orbital, solar and greenhouse gas) for 7 ka BP.

The external forcings used in the global simulation with ECHO-G are variations in Total Solar Irradiance (TSI), changes in atmospheric concentrations of greenhouse gases (GHGs), and changes in the Earth's orbit. The TSI changes were derived from the concentration of the cosmogenic isotope ^{10}Be in polar ice cores, and translated to TSI by scaling production estimates of $\delta^{14}C$ (cf. Solanki et al., 2004) such

that the difference between present-day and Maunder Minimum solar activity is 0.3 %. Past greenhouse gas concentrations were also estimated from air bubbles trapped in polar ice cores (Flückiger et al., 2002). Finally, the changes in the orbital parameters obliquity, eccentricity and position of the perihelion can be accurately calculated for the last few million years (Berger and Loutre, 1991).

The vegetation in the global model is set to present-day conditions for both simulations. Because the ECHO-G model has a very coarse resolution, vegetation changes in Europe are assumed not to have an overwhelming effect on the large scale atmospheric and oceanic circulation upstream, such as the North Atlantic Oscillation (NAO) and North Atlantic sea-surface temperatures.

2.1.2 The Rossby Centre regional atmospheric climate model RCA3

RCA3 is used to downscale results from ECHO-G to higher resolution. RCA3 and its predecessors RCA1 and RCA2 have been extensively used and evaluated in studies of present and future climate (e.g. Rummukainen et al., 2001; Räisänen et al., 2004; Kjellström et al., 2011; Nikulin et al., 2011). Also, RCA3 has been used in palaeoclimatological applications for downscaling global model results for the last millennium (Graham et al., 2009; Schimanke et al., 2012), parts of the Marine Isotope Stage 3 (Kjellström et al., 2010), and for the Last Glacial Maximum (Strandberg et al., 2011).

In RCA3, the present-day land–sea distribution and surface geopotential is used for 0.2 k. The land–sea distribution for 6 k is taken from the ICE-5G database (Peltier, 2004). The difference in orography between the two periods is caused by the changed coastline and the less detailed coastline in ICE-5G. Land and sea grid cells are therefore not exactly the same in the two periods (Fig. 1).

ECHO-G and RCA3 use the same solar irradiance. The concentrations of atmospheric GHG in RCA3 are represented as CO_2-equivalents, whereas in ECHO-G CO_2 and CH_4 are explicitly described. GHGs and solar irradiance change from year to year and are read annually by the models. Table 1 summarises the forcing from GHGs and insolation averaged over the two periods.

For snow in unforested areas, RCA3 has a prognostic albedo that varies between 0.6–0.85; the albedo decreases as snow ages. For snow-covered land areas in forest regions the albedo is set constant to 0.2. The snow-free albedo is set to 0.28 and 0.15 for unforested and forested areas, respectively. Leaf Area Index (LAI) is calculated as a function of the soil temperature with a lower limit set to 0.4, and upper limits to 2.3 (unforested) and 4.0 (deciduous forest). If deep soil moisture reaches the wilting point the LAI is set to its lower limit. LAI in coniferous forests is set constant to 4.0 regardless of soil moisture (Samuelsson et al., 2011).

RCA3 is run on a horizontal grid spacing of 0.44° (corresponding to approximately 50 km) over Europe with 24 vertical levels and a time step of 30 min. Data for initialising RCA3 are taken from ECHO-G. After that, every 12 h, RCA3 reads surface pressure, humidity, temperature and wind from ECHO-G along the lateral boundaries of the model domain, and sea-surface temperature and sea-ice extent within the model domain. All RCA3 simulations have been run for 50 yr with 1 yr spin-up time (simulated years are 3909–3861 BC for 6 k and AD 1701–1750 for 0.2 k), after which the effect of the initial conditions of atmosphere/land surface system are assumed to have faded (Giorgi and Mearns, 1999).

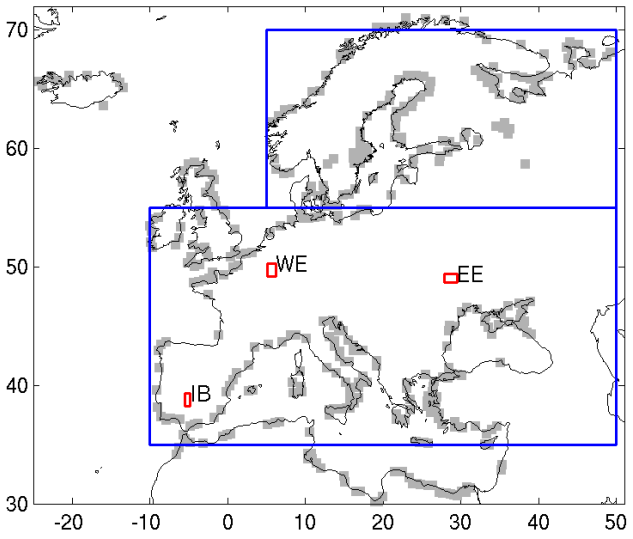

Fig. 1. Difference in land–sea distribution between 6 and 0.2 k BP; grid boxes with a difference of more than 50 % are shaded. The three regions used for analysis in Fig. 11 are marked as red squares; Iberian Peninsula (IB), western Europe (WE), eastern Europe (EE). The blue boxes represent the regions northern Europe and southern Europe described in Sect. 4.2.

For each simulation of a 50 yr period we calculate the average of the nominal seasons winter (December, January and February; henceforth DJF) and summer (June, July and August; henceforth JJA). In addition, the diurnal cycle is analysed for some regions.

The statistical significance for the difference between the simulations is determined by a bootstrapping technique (Efron, 1979). 500 bootstrap samples are used to estimate the inter-annual variability of seasonal and annual means of temperature, precipitation, latent heat flux and albedo for each simulation. The difference between two simulations is compared with the estimated distribution of a parameter (e.g. temperature) to see if the difference is statistically significant. We choose the 95 % level for significance.

2.1.3 The dynamic vegetation model LPJ-GUESS

LPJ-GUESS (Smith et al., 2001; Hickler et al., 2004, 2012) is used to simulate potential natural vegetation patterns consistent with the simulated climate in Europe during the two

selected time windows. The model has been previously used to simulate past vegetation (Miller et al., 2008; Garreta et al., 2010; Kjellström et al., 2010; Strandberg et al., 2011) and to assess the effects of land use on the global carbon cycle (Olofsson and Hickler, 2008; Olofsson, 2013).

LPJ-GUESS is a process-based dynamic ecosystem model designed for application at regional to global spatial scales. It incorporates representations of terrestrial vegetation dynamics based on interactions between individual trees and shrubs and a herbaceous understory at neighbourhood (patch) scale (Hickler et al., 2004). It accounts for the effect of stochastically recurring disturbances for heterogeneity among patches in terms of accrued biomass, vegetation composition and structure at the landscape scale. The simulated vegetation is represented by Plant Functional Types (PFTs; Table 2) discriminated in terms of bioclimatic limits to survival and reproduction, leaf phenology, allometry, life-history strategy and aspects of physiology governing carbon balance and canopy gas-exchange. Differences between PFTs in combination with the present structure of the vegetation in each patch govern the partitioning of light and soil water among individuals as well as regeneration and mortality, affecting competition among PFTs and age/size classes of plants.

Inputs to the model are temperature (°C), precipitation (mm), net downward short-wave radiation at surface ($W\,m^{-2}$) and wet day frequency (days), all in monthly timesteps provided by RCA3 at a 0.44° spatial resolution over Europe and annual atmospheric CO_2 concentration for the 6 and 0.2 k time windows. The static, present-day soil texture data described in Sitch et al. (2003) were used during all simulations. The PFT determination was based on the European dominant species version described by Hickler et al. (2012) (Table 2).

2.1.4 The anthropogenic land cover change scenarios KK10 and HYDE3.1

The historical ALCC scenarios most often used in earth system modelling are HYDE3.1 (Klein Goldewijk et al., 2011), KK10 (Kaplan et al., 2009) and the scenarios of Pongratz et al. (2009b). We have chosen HYDE3.1 and KK10 for this study because they represent the two extremes of estimated anthropogenic impact at the two selected time windows. These ALCC models use similar estimates of past human population density, but differ in their estimates of land requirement per capita and the assessment of the effect of contrasting technological development between regions. Therefore, they provide substantially different scenarios of the extent of deforestation and land-use intensity (Gaillard et al., 2010; Boyle et al., 2011; Kaplan et al., 2011).

KK10 represents the total amount of the land fraction used for agrarian activities at a 5′ spatial resolution. The HYDE3.1 (hereafter referred to as H3.1, HYDE, 2011) land-use data set includes information on the fraction of cropland, grassland and urban areas, also at a 5′ spatial resolution. The different land-use categories are summed up to represent the total fraction of anthropogenic deforestation. Upscaled (averaged to a 0.5° resolution) versions of both data sets for the two selected time windows are used as input in the RCM runs (Fig. 2).

While proxy-based quantitative information on anthropogenic land use before the 20th century is rare, KK10 and HYDE3.1 have been evaluated in western Europe north of the Alps (the LANDCLIM project study region) using pollen-based quantitative reconstructions of vegetation cover based on the "Regional Estimates of VEgetation Abundance from Large Sites" (REVEALS) model (Sugita, 2007). REVEALS is a mechanistic model of pollen dispersal that can reduce biases caused by inter-taxonomic differences in pollen productivity and dispersal/deposition characteristics properties. The comparison of KK10 and HYDE3.1 with the REVEALS-model estimates of open land for five time windows of the Holocene – 6000, 3000, 600, 200 cal yr BP and recent past (LANDCLIM vegetation data set; Gaillard, 2013; Trondman et al., 2013) – shows that the KK10 scenarios tend to be more similar to the REVEALS-based reconstruction of vegetation cover than the HYDE3.1 scenarios (Kaplan et al., 2014). The REVEALS estimates of open land for the two time windows used in this study are shown in Fig. 2 for comparison.

2.2 Alternative land-cover descriptions used in the RCA3 runs

Potential natural land cover (hereafter referred to as V) for 6 and 0.2 k is simulated using LPJ-GUESS (forced with results from RCA3). The resulting LAI per PFT and per grid cell is averaged over the modelling period for both time windows and then converted to foliage projective cover (FPC). The FPC is defined, applying the Lambert–Beer law (Monsi and Saeki, 1953), as the area of ground covered by foliage directly above it (Sitch et al., 2003):

$$\mathrm{FPC(PFT)} = 1.0 - \exp(-k * (\mathrm{LAI(PFT)})),$$

where k is the extinction coefficient (0.5).

The calculated species-specific FPC-values were summed up to three RCA3-specific PFTs (Table 2) per grid cell. The fraction of non-vegetated land is calculated by subtracting the sum of all the PFT-values per grid cell from one.

In order to obtain a description of the land cover including information on both natural and human-induced vegetation the LPJ-GUESS simulation results (V) are combined with the two ALCC simulations, KK10 and H3.1. The V + KK10 and V + H3.1 vegetation descriptions are constructed by subtracting the ALCC fraction determined by KK10 or H3.1 from one, and thereafter homogeneously rescaling the PFT values provided by V in all grid cells to fit into the remaining space. The total unforested fraction is then calculated by summing up the ALCC KK10 or H3.1 with the LPJ-GUESS simulated PFT Grass fractions in each grid cell.

Table 2. The three plant functional types (PFTs) for regional climate model RCA3; LPJ-GUESS PFTs according to Hickler et al. (2012) and Wolf et al. (2008); LANDCLIM REVEALS taxa (Mazier et al., 2012); and modern analogue technique (MAT) PFTs adapted from Peyron et al. (1998).

RCA3 PFT	LPJ-GUESS PFT	LANDCLIM REVEALS taxa*	MAT PFT
Coniferous tree canopy	*Picea_abies*	*Picea*	Boreal evergreen/ cool-temperate conifer
	Abies_alba	*Abies*	
	Pinus_sylvestris, P. halepensis	*Pinus*	
	Tall shrub evergreen, *Juniperus oxycedrus*	*Juniperus*	Eurythermic conifer
			Boreal summergreen
			Intermediate temperate
Broad-leaved tree canopy		*Alnus*	Temperate/boreal summergreen/arctic-alpine
	Betula pendula, B. pubescens	*Betula*	Boreal summergreen arctic-alpine
	Corylus avellana	*Corylus*	Cool-temperate summergreen
	Carpinus betulus	*Carpinus*	
	Fagus sylvatica	*Fagus*	
	Fraxinus excelsior	*Fraxinus*	Temperate summergreen
	Mediterranean rain green shrub		
	Populus tremula		Temperate/boreal summergreen
	Quercus coccifera, Q. ilex	*Quercus*	Warm-temperate broad-leaved evergreen
	Quercus pubescens, Q. robur		Temperate summergreen
	Tilia cordata	*Tilia*	Cool-temperate summergreen
	Ulmus glabra	*Ulmus*	
	Tall shrub summergreen	*Salix*	Temperate/boreal summergreen/arctic-alpine
			Warm-temperate summergreen
			Cool-tremperate broad-leaved evergreen
			Warm-temperate
			Warm-temperate sclerophyll trees/shrub
Unforested	C3 Grass	Cereals (*Secale* excluded) /Cerealia-t, *Secale*, *Calluna*, *Artemisia*, Cyperaceae, *Filipendula*, *Plantago lanceolata*, *P. montana*, *P. media*, Poaceae, *Rumex p.p.* (mainly *R. acetosa R. acetosella*)/*R. acetosa*-t	Non arboreal

* These taxa have specific pollen-morphological types. When the latter correspond to a botanical taxon, they have the same name; if not, it is indicated by the extension "-t".

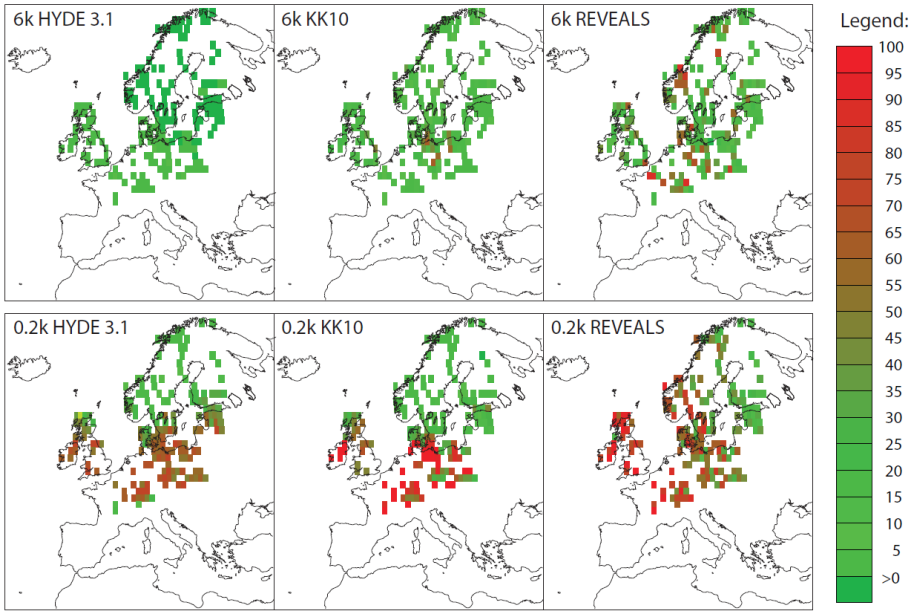

Fig. 2. The anthropogenic land-use scenarios HYDE3.1 (Klein Goldewijk et al., 2011) and KK10 (Kaplan et al., 2009), and the grid-based (GB) REVEALS reconstructions (Trondman et al., 2013) at 6 and 0.2 k BP and a spatial scale of 1'. The colour coding represents the degree of human-induced deforestation in % cover (HYDE3.1 and KK10) and the % cover of plants characteristic of grassland (primarily grasses, sedges, sorrel and a few other herbs) and cultivated land (cereals) as estimated by the REVEALS model using pollen data. Reddish to red colours represent > 50 % deforestation, and green colours < 50 % deforestation, These maps are not directly comparable as the methods used in the model scenarios follow a totally different approach, and the REVEALS-based reconstructions represent actual openness, natural and human-induced (see method section for more details). Nevertheless, these maps show that in several areas of Europe, in particular western Europe (e.g. Britain, France, Switzerland, Germany), the KK10 scenarios are closer to the pollen-based REVEALS reconstructions than the HYDE3.1 scenarios in terms of intensity of human land use, given that there was little natural openness at 6 k and most of the openness at 0.2 k was human induced. A more in-depth/sophisticated comparison of these scenarios and the REVEALS reconstructions are discussed in detail in Kaplan et al. (2014).

The simulated V, V + H3.1 and V + KK10 land-cover descriptions are recalculated to 100 % vegetation, omitting the non-vegetated fraction and upscaled to a 1° spatial resolution. The agreement of the three sets of results is assessed by comparison of the dominant (> 50 %) land cover type (unforested or forested) between the sets.

2.3 Proxy data of past climate

We use two proxy data sets of past climate for comparison with the RCA3 climate simulations at 6 and 0.2 k: the LANDCLIM database of past climate proxy records, consisting mainly of site specific/point reconstructions of past climate based on non-pollen proxies (Nielsen et al., 2014); and the spatially explicit pollen-based climate reconstruction of Mauri et al. (2013). The LANDCLIM project itself is concerned about circular reasoning and avoids using climate reconstructions based on pollen records because the REVEALS reconstructions of vegetation cover are also based on pollen records (see below). Nevertheless, in this study, we chose to also use a pollen-based reconstruction of climate for Europe because it is the only spatially explicit description of past climate existing to date, keeping in mind, however, that the pollen data used might bias the climate reconstruction due to significant human-induced changes in vegetation from ca. 3 k (e.g. Gaillard, 2013) (see discussion). For the southern and eastern parts of the study area covered by the RCA3 simulations but not by the LANDCLIM database, we rely primarily on the non-pollen proxy-based climate reconstructions presented in Magny and Combourieu Nebout (2013), and in particular the synthesis of palaeohydrological changes and their climatic implications in the central Mediterranean region and its surroundings (Magny et al., 2013). The Mauri et al. (2013) reconstruction in the Mediterranean area is also compared to the pollen-based climate reconstructions in the Mediterranean region published by Peyron et al. (2013). The latter reconstructions are based on the multi-method approach that uses a combination of pollen-based weighted averaging, weighted-average partial least-squares regression, modern analogue technique (MAT), and non-metric multidimensional scaling/generalized additive model methods.

The LANDCLIM database of past climate records includes data sets of palaeoecological proxies, data from written archives and instrumental measurements from 245 sites in western Europe north of the Alps for the two time

windows 6 k (5700–6200 BP) and 0.2 k (AD 1700–1800) as well as for the time after AD 1960. Climate reconstructions based on proxies of vegetation (plant macrofossils and pollen) are excluded from the database to avoid circular reasoning. The selected reconstructions are dated with multiple radiocarbon dates of terrestrial plant material, varve counts, dendrochronology, TIMS (thermal ionisation mass spectrometry)-dated speleothems or historical records. To compare our model-simulated climate results with empirical climate reconstructions, we used primarily the proxies based on diatoms, tree rings and chironomids for summer temperatures (July T), and proxies based on lake-level changes, varve thickness in lake sediments, and ^{13}C and ^{18}O in carbonates for relative changes in yearly precipitation minus evaporation (P-E).

The climate reconstruction of Mauri et al. (2013) largely follows the modern analogue technique (MAT) approach described in Davis et al. (2003), but it is based on much improved pollen data sets. The modern surface sample data set was compiled from the European Modern Pollen Database (Davis et al., 2013) and represents a substantial improvement compared to that used in Davis et al. (2003), with an increase in the number of samples by $\sim 80\,\%$ (total of 4287 sites). The fossil data set includes 48 % more sites (total of 756 sites) compared with Davis et al. (2003), with this improvement in data coverage spread throughout Europe. The MAT approach calculates a pollen–climate transfer function to reconstruct palaeoclimate from fossil pollen data, where the fossil and modern pollen samples are matched using pollen assemblages grouped into PFTs (Table 2). The use of PFT groups allows a wider range of taxa to be included in the analysis without over-tuning the transfer function, and allows taxa to be included that may not be present in the modern pollen calibration data set. Since PFT groups are largely defined according to their climatic affinities (Prentice et al., 1996), the approach also reduces the sensitivity of the transfer function to non-climatic influences, such as human impact on vegetation, disease, ecological competition or succession, or soil processes. Approximate standard errors for the reconstruction were calculated following Bartlein et al. (2010) by assimilating samples at the interpolated spatial grid resolution, together with the standard error from the interpolation itself.

3 Results

3.1 LPJ-GUESS simulated vegetation

The simulated potential vegetation (V) at 6 k is characterised by a forest cover of $> 90\,\%$ in most of Europe (Fig. 3). The areas with less than 50 % of forest cover (central Alps, Scandinavian mountains, northern Scandinavia and Iceland) are typically related to high elevations and/or latitudes. The simulated forest composition of northern and eastern Europe and elevated areas of central Europe is dominated by coniferous trees, while western and lowland Europe is dominated by broad-leaved trees. The average HYDE3.1 anthropogenic land cover/deforestation (H3.1) at 6 k is generally $< 1\,\%$; values $> 5\,\%$ are restricted to some areas of southern Europe (Fig. 3). Therefore, the V + H3.1 land cover description does not differ markedly from V. The KK10 estimates of deforestation are higher ($> 4\,\%$ in average) and reach values $> 50\,\%$ in southern Europe and restricted areas of southern Scandinavia, Belgium and the northern Alps. However, the additional unforested land predicted by HYDE3.1 and KK10 is negligible in comparison to the potential unforested land simulated by LPJ-GUESS, which explains why the V, V + H3.1 and V + KK10 land cover descriptions do not differ significantly from each other at 6 k.

The V land-cover description at 0.2 k shows little difference compared to V at 6 k (Fig. 3). The largest differences are found in Scandinavia where areas with less than 50 % of forest cover are much larger than they are at 6 k. The average H3.1 estimates of deforestation are ca. 10 %, but reach values $> 50\,\%$ in southern Europe. The KK10 estimates of anthropogenic deforestation are $> 40\,\%$ on average and the highest values ($> 95\,\%$) are found in southern Europe. Owing to the high KK10 estimates in most of western, central and southern Europe, the forest cover is considerably reduced in V + KK10 in comparison to V + H3.1 and particularly to V.

3.2 Simulated climate

The overall features of the simulated 6 and 0.2 kV regional climate are comparable. Winter (DJF) mean temperatures range from $-15\,^{\circ}C$ in northern Europe to $10\,^{\circ}C$ over the Iberian Peninsula (Figs. 4 and 5, upper left panels). In summer (JJA), the highest temperatures (ca. $20\,^{\circ}C$) occur in the Mediterranean region, while summer mean temperatures do not reach more than ca. $10\,^{\circ}C$ in northern Scandinavia (Figs. 4 and 5, lower left panel). Summer temperatures at 6 k are ca. 0–2 °C warmer than at 0.2 k in most of Europe (Fig. 6). In winter, northern Europe is 1–2 °C warmer at 6 k than at 0.2 k, while large parts of central Europe are ca. 0.5 °C colder.

The largest precipitation amounts in winter (100–150 mm month^{-1}) fall in the western parts and mountain ranges of the study area, while the smallest amounts (30–60 mm month^{-1}) are found in the eastern regions (Figs. 7 and 8, top rows). In summer, most precipitation (60–100 mm month^{-1}) falls over the land areas of the northern half of Europe, and the least around the Mediterranean (0–50 mm month^{-1}) (Figs. 7 and 8, bottom rows). The only significant differences in precipitation are seen in summer in parts of eastern and central Europe where 6 kV is drier than 0.2 kV by 10–20 mm month^{-1} (Fig. 9).

The difference between the simulated V climate and the V + H3.1 or V + KK10 climate at 6 k is generally not statistically significant, but the V + KK10 climate exhibits a few hotspots (southern Scandinavia, Belgium, north of

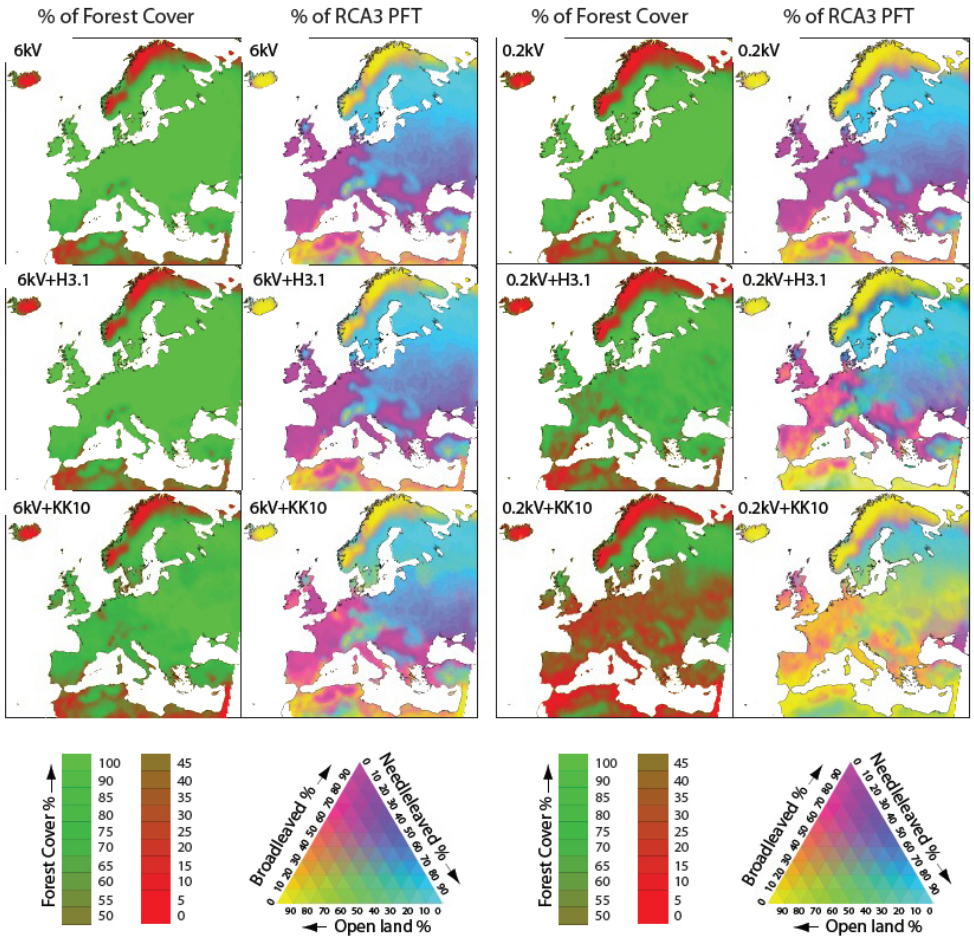

Fig. 3. Proportion of the LPJ-GUESS simulated potential natural vegetation cover (V) represented by fraction of forest (columns 1 and 3) and three RCA3 PFTs (i.e. broad-leaved trees, needle-leaved trees and unforested) (columns 2 and 4) at 6 k BP (columns 1 and 2) and 0.2 k BP (columns 3 and 4). The simulation is forced by the initial RCA3 model-simulated climate. The simulated vegetation cover (V) is post-processed by overlaying the anthropogenic deforestation scenarios from the HYDE 3.1 database (Klein Goldewijk et al., 2010) (V + H3.1) and the KK10 scenarios of Kaplan et al. (2009) (V + K). The colour scales indicates the fractions of forest and the PFTs within each grid box.

the Alps) with summer temperatures 0.5–1 °C warmer than the V simulation (Fig. 4). Winter precipitation hardly differs between the 6 k V, V + H3.1 and V + KK10 simulations, whereas small but statistically significant differences in summer precipitation (not more than -10 mm month^{-1}) between the 6 k V + KK10 simulation and the other two 6 k simulations are found mostly in central Europe (Fig. 7). The unchanged precipitation pattern during winter in between the different RCA3 simulations might be due to the large influence of the large-scale atmospheric circulation during winter, inheriting the information from ECHO-G into RCA3. During summer this effect is much less, and more regional-to-local scale effects influence precipitation patterns.

At 0.2 k, deforestation (V + H3.1 and V + KK10) leads to lower winter (DJF) temperatures than potential vegetation (V) (Fig. 5, top row). The lower temperatures are confined to the Alps and parts of eastern Europe in the V + H3.1 simulation, while they are found in all of eastern Europe and southern Scandinavia in the V + KK10 simulation, in some regions with as much as a 1–1.5 °C difference between the V + KK10 and V simulations. However, the winter temperature differences between all simulations are statistically significant only in parts of eastern Europe. Summer (JJA) temperatures at 0.2 k are also lower (Fig. 5, bottom row), but only in the Mediterranean region, again most pronounced in the V + KK10 simulation. Conversely, higher summer temperatures by up to 1 °C in parts of eastern Europe are a particular feature in the V + KK10 simulation at 0.2 k. Summer precipitation is lower by 0–20 mm month^{-1} in scattered parts of central and southern Europe in the V + H3.1 simulation at 0.2 k, while it is lower in all regions where the simulated forest fraction is reduced by more than 50 % in the V + KK10 simulation, with statistically significant differences of -10 to -30 mm month^{-1} in most of Europe (Fig. 8). Differences in winter precipitation between the simulations are very small.

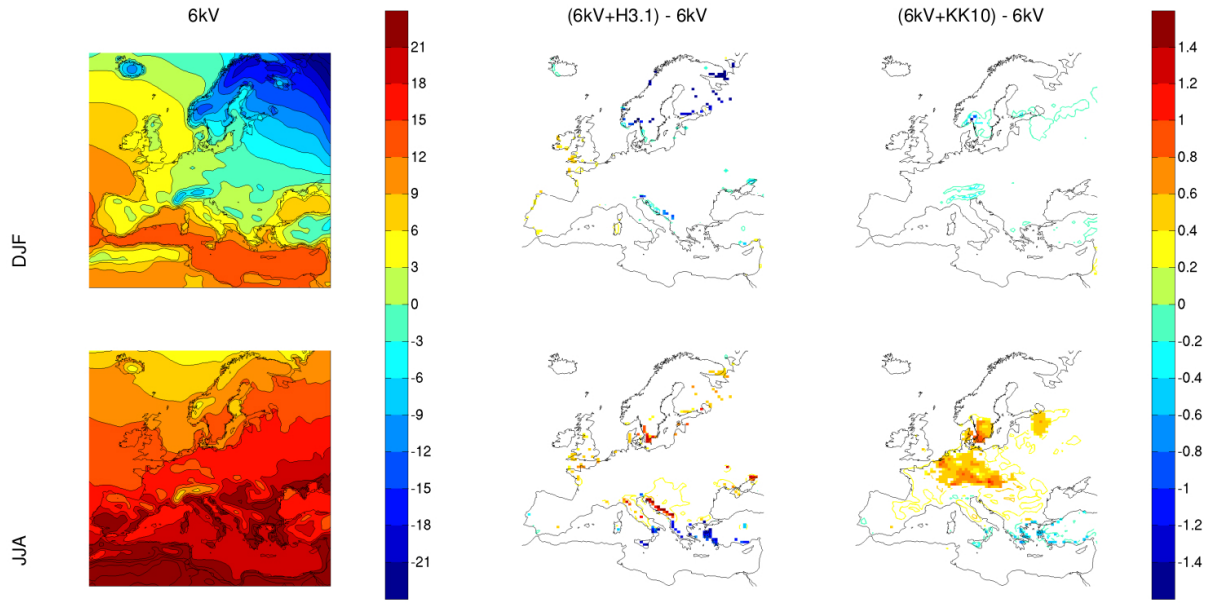

Fig. 4. Temperature (°C) at 6 k BP for winter (top row) and summer (bottom row). Absolute temperature from run 6 kV (left), difference 6 kV + H3.1–6 kV (middle) and 6 kV + KK10–6 kV (right). In the middle and right panels, grid boxes with a significant temperature difference at the 95 % level are coloured. Isolines show changes in the remaining regions. The "zero isoline" is excluded.

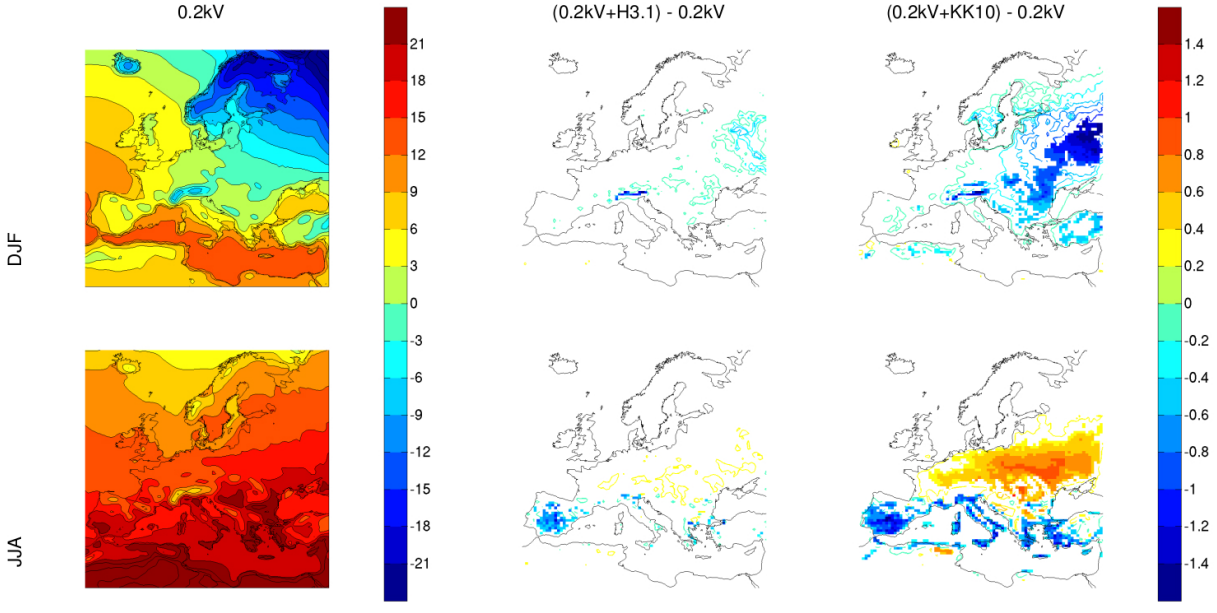

Fig. 5. Temperature (°C) at 0.2 k BP for winter (top row) and summer (bottom row). Absolute temperature from run 0.2 kV (left), difference 0.2 kV + H3.1–0.2 kV (middle) and difference 0.2kV + KK10–0.2kV (right). In the middle and right panels, grid boxes with a significant temperature difference at the 95 % level are coloured. Isolines show changes in the remaining regions. The "zero isoline" is excluded.

The difference between the 6 and 0.2 k simulations (6–0.2 k) greatly depends on the vegetation description used in the climate model runs, i.e. V, V + H3.1 or V + KK10 (Figs. 6 and 9). The climate simulations using vegetation descriptions with high values of deforestation (V + KK10) yield larger 6–0.2 k differences in summer temperature in south-west Europe (by 1–2 °C higher) than in eastern Europe (by ca. 1 °C). High values of deforestation at 0.2 k yield larger differences in (i) winter temperatures in eastern Europe (by 1–2 °C higher at 0.2 k than at 6 k), while small or no differences are seen in the rest of Europe (Fig. 6), and (ii) summer precipitation in south-east Europe (by around

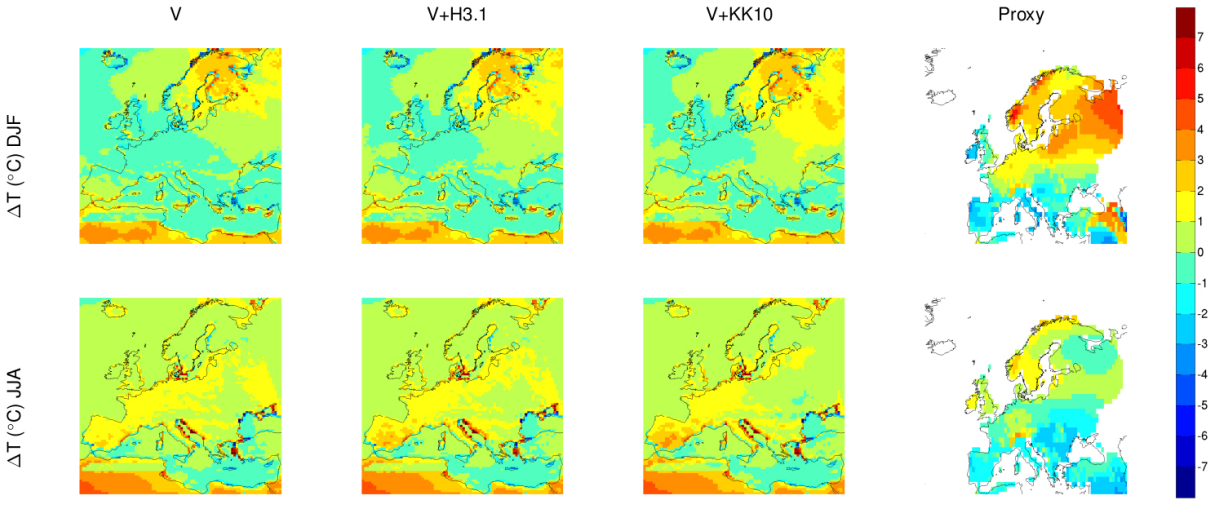

Fig. 6. Difference between RCA3 runs at 6 and 0.2 k BP (6–0.2 k) (columns 1–3) and pollen-based reconstruction (column 4) for temperature (ΔT, °C) in winter (DJF, top row) and summer (JJA, bottom row). Note that the map projection differs from the model results and proxy estimates.

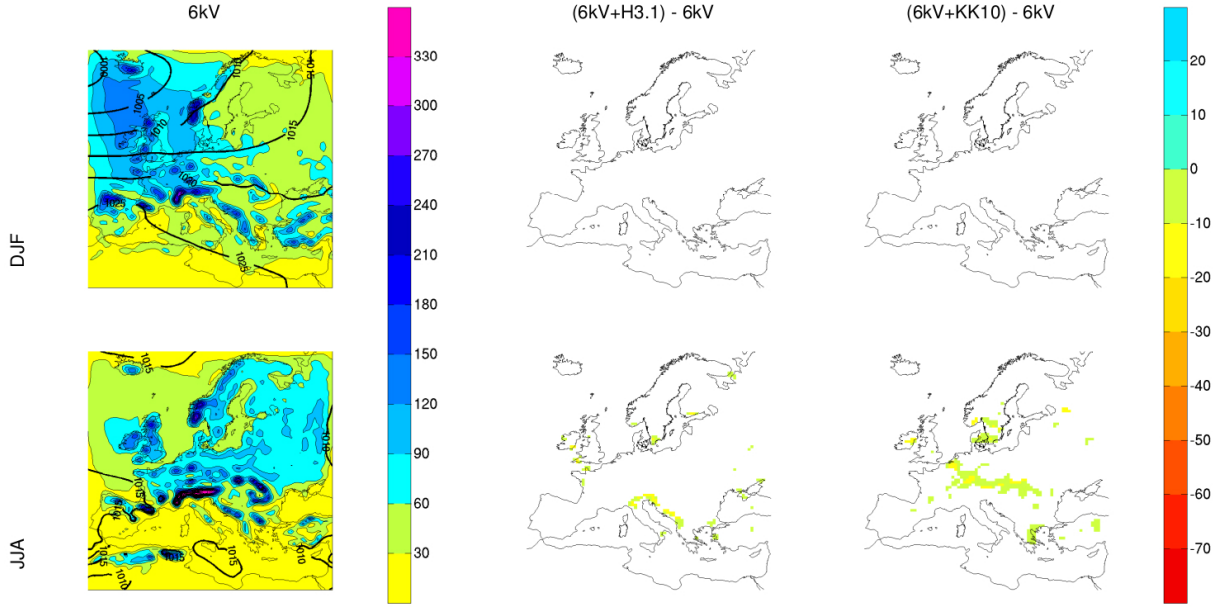

Fig. 7. Precipitation (mm month^{-1}) at 6 k BP for winter (top row) and summer (bottom row). Absolute precipitation and pressure from run 6 kV (left), difference 6kV + H3.1–6 kV (middle) and difference 6kV + KK10–6 kV (right). In the left panels isolines indicate pressure (hPa). In the middle and right panels grid boxes with a significant precipitation difference at the 95 % level are coloured. Isolines show differences in the remaining regions. The "zero isoline" is excluded.

30 mm month^{-1} higher at 0.2 than 6 k). In contrast, large deforestation at 0.2 k leads to smaller differences in winter precipitation between 0.2 and 6 k in central Europe (Fig. 9).

The general effect of changes in the extent of deforestation on the simulated climate is a change in the amplitude in temperature and/or precipitation differences between 6 and 0.2 k rather than a change in the geographical pattern of those differences.

3.3 Climate response to land-use changes

The largest differences in seasonal mean temperature and precipitation between the RCA3 simulations are found at 0.2 k between the V and V + KK10 simulations. In order to assess the processes behind land cover–climate interactions, we analyse the annual cycle of temperature and latent heat flux at 0.2 k for three regions with particularly large deforestation but different climate responses (see section above):

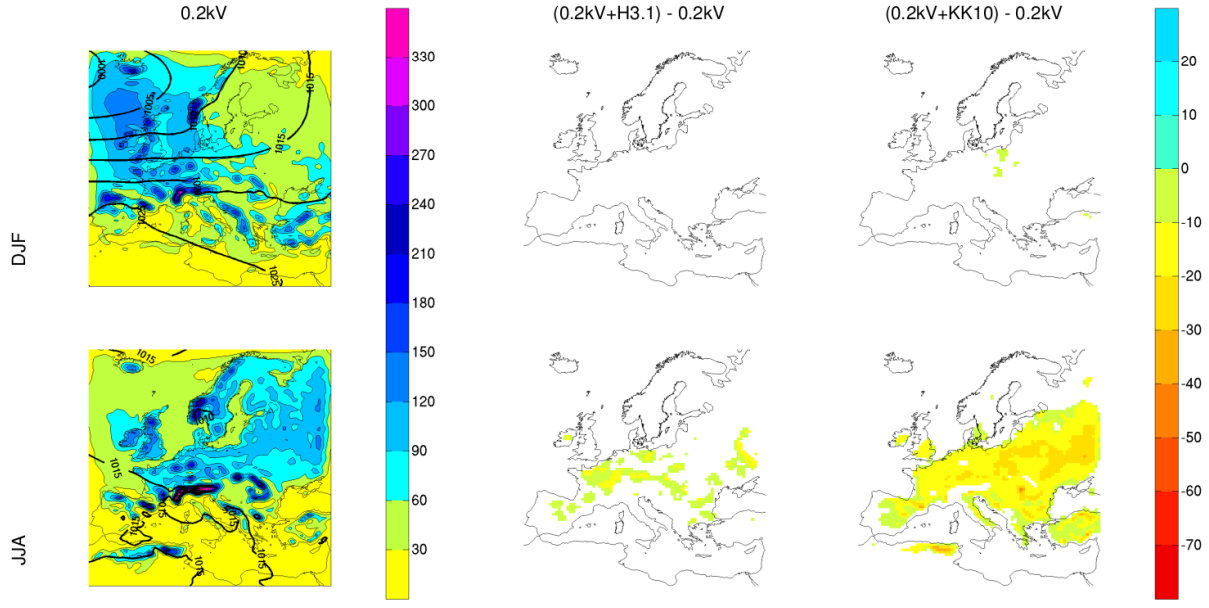

Fig. 8. Precipitation (mm month^{-1}) at 0.2 k BP for winter (top row) and summer (bottom row). Absolute precipitation and pressure from run 0.2 kV (left), difference 0.2kV + H3.1–0.2 kV (middle) and difference 0.2kV + KK10–0.2 kV (right). In the left panels isolines indicate pressure (hPa). In the middle and right panels grid boxes with a significant precipitation difference at the 95 % level are coloured. Isolines show differences in the remaining regions. The "zero isoline" is excluded.

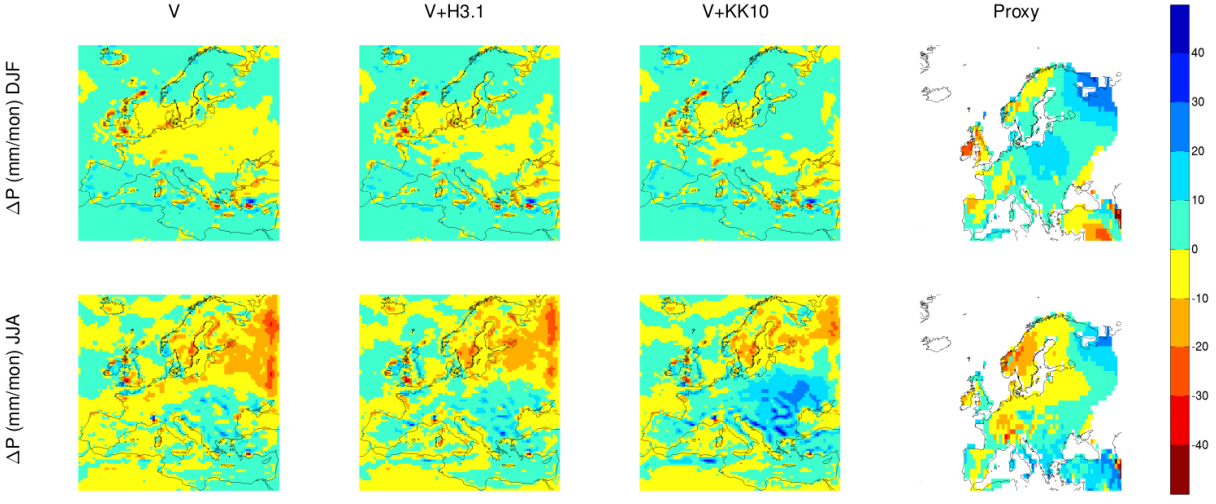

Fig. 9. Difference between RCA3 runs at 6 and 0.2 k BP (6–0.2 k) (columns 1–3) and pollen-based reconstruction (column 4) for precipitation (ΔP, mm month^{-1}) in winter (DJF, top row) and summer (JJA, bottom row). Note that the map projection differs from the model results and the proxy estimates.

western Europe (WE), eastern Europe (EE) and the Iberian Peninsula (IB). For each region, 3 × 3 grid boxes are selected (Fig. 1).

In winter, lower temperatures due to deforestation are best explained by the albedo effect. The albedo is highest in the V + KK10 simulation since low herb vegetation has a higher albedo than forests (Fig. 10, left column). The difference in albedo is even higher during the snow season, since unforested areas are more readily covered by snow. Moreover, the effect increases in late winter/spring because of more incoming sunlight. Hence, deforestation leads to larger differences in winter temperature in the north/east, where the snow season is longer, than in the west/south.

When vegetation starts to be active in spring, the albedo effect is counteracted by differences in latent heat flux. Generally, the larger biomass of forests compared to low vegetation

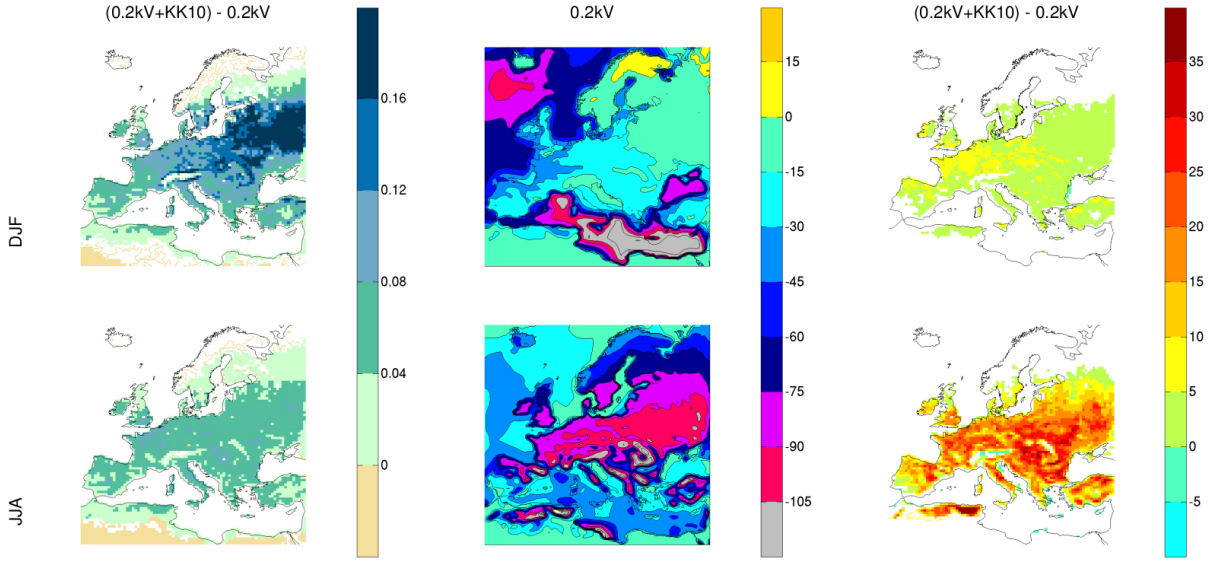

Fig. 10. Albedo difference, 0.2kV + KK10–0.2 kV (left), absolute latent heat flux (W m^{-2}) from run 0.2 kV (middle), and difference in latent heat flux 0.2kV + KK10–0.2 kV (right) for winter (top) and summer (bottom). In the left and right panels, grid boxes with a significant difference at the 95 % level are coloured. Isolines show differences in the remaining regions. The "zero isoline" is excluded.

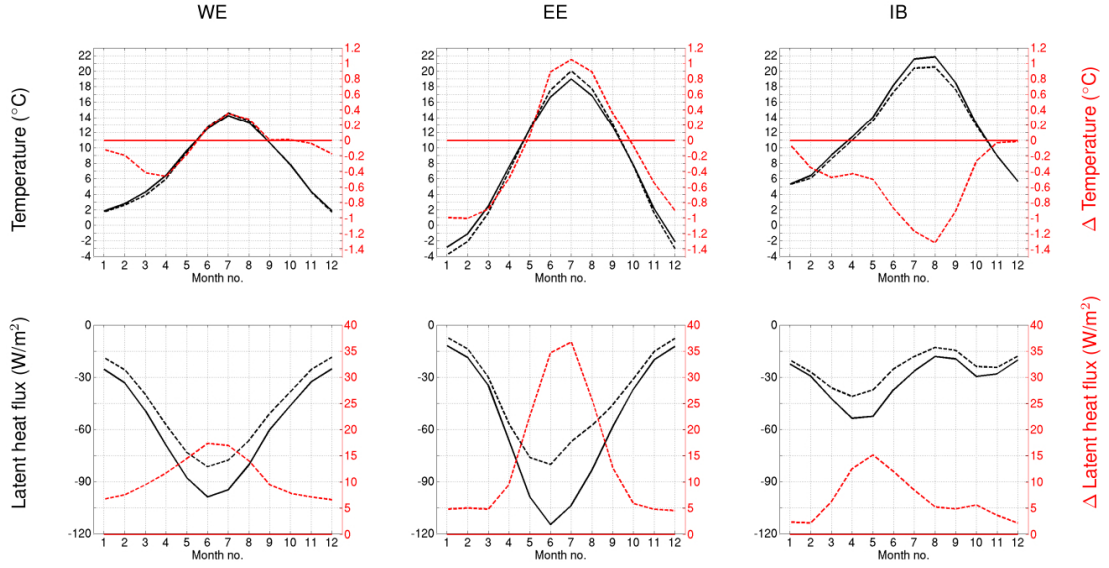

Fig. 11. Annual cycles of temperature (°C, top row) and latent heat flux (W m^{-2}, bottom row) for locations in western Europe (WE), eastern Europe (EE) and Iberian Peninsula (IB). Black lines show absolute values and red lines show anomalies relative to 0.2 kV. Full black line: 0.2 kV; dashed black line: 0.2kV + KK10; full red line: 0.2 kV–0.2 kV (i.e. zero difference); dashed red line: 0.2kV + KK10–0.2 kV. Definitions of WE, EE and IB are found in Fig. 1.

leads to more evapotranspiration and, consequently, lower temperatures in forested than in deforested regions (Fig. 10, centre and right columns). The differences between the two simulations in latent heat flux start earlier in the year in WE compared to EE (Fig. 11, bottom row). Moreover, latent heat flux is weaker in summer and the difference between the V + KK10 and V simulations is smaller in WE than in EE, which explains the relatively moderate temperature difference between the two simulations in summer for WE. WE is also much influenced by the large-scale weather systems from the Atlantic, which makes changes in the regional surface properties less important than in EE. The latent heat flux in IB is strongest already in spring. When soils are dry in summer, the latent heat flux is weak and, therefore, the difference between the V + KK10 and V simulations is small.

In that case, the change in albedo dominates over the change in latent heat flux, leading to lower summer temperatures.

Differences in precipitation also correlate with differences in latent heat flux (Figs. 8 and 10). Since differences in precipitation are caused primarily by a change in convective precipitation (not shown), it suggests that convective precipitation also changes as a result of deforestation. This would explain that 0.2 k is drier in EE than 6 k in the V + KK10 simulations. Observations in the tropics have indeed shown that regional deforestation decreases precipitation (Spracklen et al., 2012).

4 Discussion

4.1 Comparison of the RCA3-simulated regional climate with palaeoclimate reconstructions

Studies of diatoms (Korhola et al., 2000; Rosén et al., 2001; Bigler et al., 2006), tree rings (Grudd, 2002; Helama et al., 2002) and chironomids (Rosén et al., 2001; Bigler et al., 2003; Hammarlund et al., 2004; Laroque and Hall, 2004; Velle et al., 2005) indicate a 6–0.2 k difference in summer temperature of 0.5–2 °C in Scandinavia, which agrees with our simulations. Evidence from the presence of Mediterranean ostracods in the coastal waters of Denmark suggests that winter temperature at 6 k were up to 4–5 °C above present (Vork and Thomsen, 1996). Proxy records of relative precipitation indicate a drier climate at 6 k than at 0.2 k in Scandinavia (Digerfeldt, 1988; Ikonen, 1993; Snowball and Sandgren, 1996; Hammarlund et al., 2003; Borgmark, 2005; Olsen et al., 2010), northern Germany (Niggeman et al., 2003) and the UK (Hughes et al., 2000), while there is no detectable difference in the Alps (Magny, 2004). Our simulations show similar general features (Figs. 6 and 9). Unfortunately, quantitative proxy-based temperature estimates are mainly available for Scandinavia where differences between the simulated climates with alternative land-use scenarios are small. Therefore, none of the simulated climates agrees significantly better with the proxies than the others.

In the Mediterranean region, independent non-pollen proxy-based data indicate contrasting patterns of palaeohydrological changes between the regions north and south of the ca. 40° N latitude (Magny et al., 2013). The proxies imply that 6 k (0.2 k) were dry (wet) north of 40° and wet (dry) south of 40°. The available data in the synthesis of Magny et al. (2013) also suggest that these contrasting palaeohydrological patterns operated throughout the Holocene, both on millennial and centennial scales. Moreover, the combination of lake-level records and fire data was shown to provide information on the summer moisture availability. Fire frequency depends on the duration and intensity of the dry season (Pausas, 2004; Vannière et al., 2011), while the main proxies used in lake-level reconstructions are often related to precipitation during the warm season (dry in summer; Magny, 2007). The fire records published by Vannière et al. (2011) indicate the same contrasting pattern between the north- and the south-western Mediterranean for the Mid-Holocene (including 6 k), with dry summers in the north and humid summers in the south. The evidence presented in Magny et al. (2013) suggests that, in response to centennial-scale cooling events, drier climatic conditions developed in the south-central Mediterranean, while wetter conditions prevailed in the north-central Mediterranean. In general, the centennial phases of higher lake-level conditions in west-central Europe were shown to coincide with cooling events in the North Atlantic area (Bond et al., 2001; e.g. Magny, 2004, 2007) and decreases in solar activity before 7 k, and with a possible combination of NAO-type circulation and solar forcing since ca. 7 k onwards.

The 6–0.2 k difference in the simulated climate is generally small for all simulations (V, V + H3.1 and V + KK10) compared to the 6–0.2 k differences in the pollen-based climate reconstructions (PB reconstructions). Moreover, the geographical/spatial patterns of these 6–0.2 k differences show discrepancies between simulations and reconstructions (Fig. 6). The difference in summer temperatures ranges from ca. +1 °C in Scandinavia to ca. −2 °C in southern Europe in the PB reconstructions, while it is ca. +2–3 °C in southern and central Europe and ca. +1 °C in northern and eastern Europe in the RCA3 simulations. The difference in winter temperatures in the PB reconstructions ranges from ca. −3 °C in southern Europe and ca. +3 °C in northern Europe, while the RCA3 simulations show a different pattern, with differences ranging from +2–3 °C in Scandinavia to around 0 °C in central Europe and ca. +1 °C in southern Europe. The difference in insolation in summer between 6 and 0.2 k is positive in all of Europe, but the difference is larger in northern Europe (see Fig. 2 in Wagner et al., 2007). When considering astronomical forcing alone, we would expect 6 k to be warmer than 0.2 k and the temperature difference to be largest in summer in northern Europe. This is the signature we see in the model simulations. The non-pollen proxy based palaeoclimatic data presented above and the pollen based reconstruction of Peyron et al. (2013) rather support the differences in summer temperatures simulated by RCA3 than the PB reconstruction of Mauri et al. (2013), in particular for southern and eastern Europe. For the winter temperatures, we have no appropriate non-pollen proxy based data to evaluate the RCA3 and PB results. Of the three RCA3 simulations, the V + KK10 is the one that is closest to the PB reconstruction, which would imply that the description of land cover V + KK10 is closest to the actual vegetation at 0.2 k and therefore the V + KK10 simulated climate is closer to the PB reconstruction.

The RCA3 simulations and the PB reconstructions both show a drier climate in summer at 6 k than at 0.2 k in northern and western Europe and a wetter climate in south-eastern Europe, but they disagree in eastern/north-eastern Europe where the RCA3 simulations indicate drier summer conditions at 6 k than at 0.2 k, while the PB reconstructions show

wetter summer conditions at 6 k than at 0.2 k (Fig. 9). In terms of winter precipitation, the RCA3 simulations and the PB reconstructions display entirely different results. According to RCA3, winter precipitation is not significantly different between 6 and 0.2 k in most of Europe, while the PB reconstructions indicate wetter conditions at 6 k than at 0.2 k in central and eastern Europe and drier in western Europe. We have no quantitative proxy records (other than pollen-based reconstructions) available to evaluate the RCA3 results for summer temperatures in eastern Europe and winter precipitation in the entire study region.

The two climate regions identified by Magny et al. (2013) are not seen in the PB reconstructions of Mauri et al. (2013) and the RCA3 simulations, except for a weak pattern of contrasting summer temperatures on both side of latitude 40° N in the RCA3 simulations. However, it should be noted that 6 k is within the transition period (6.4–4.5 k) between the two climate regimes before and after 4.5 k described by Magny et al. (2013), which may explain that the patterns around 6 k are difficult to capture both by the climate model and the PB reconstructions. Also, there is a general problem of accurately disentangling multiple climatic variables from the fossil pollen data, which causes uncertainties in the PB reconstruction. Further, there is no equivalent in the non-pollen proxy-based palaeoclimatic records to the PB reconstruction of Mauri et al. (2013) in terms of higher winter precipitations at 6 k than at 0.2 k in eastern Europe north of 40° N.

The comparison between climate model simulations and pollen-based palaeoclimate data indicates that discrepancies occur in the geographical patterns of the differences in climate between 6 and 0.2 k. This is particularly clear for temperatures in southern Europe, where model and proxies exhibit opposite signs of the difference in temperature, and for winter precipitation, where reconstructions exhibit much larger differences than the RCA3 simulations (Figs. 6 and 9). A wetter summer in western central Europe at 0.2 k than at 6 k is in better agreement with the non-pollen proxy records (e.g. in the Jura mountains; Magny et al., 2013) than a drier western central Europe as indicated in the PB reconstruction.

As the differences between the three model simulations (V, V + H3.1 and V + KK10) are generally smaller than the differences between the model simulations and the pollen-based reconstructions of past climate, it is not possible to identify the vegetation description (V, V + H3.1 or V + KK10) that provides the most coherent simulated climate for Europe at 6 and 0.2 k.

4.2 Model simulations in a wider perspective

In this study, we use boundary conditions provided by the GCM ECHO-G. ECHO-G is one of many GCMs and the use of boundary conditions from another GCM may give different RCA3 results. Moreover, a different realisation of the climate with ECHO-G would likely result in a different RCA3 output as the impact of internal variability is large (Deser et al., 2012). In order to assess to what degree our results might be biased by the choice of one single GCM realisation, we compare our results with an ensemble of PMIP models. This ensemble represents uncertainties related both to the choice of GCM and to internal variability as each GCM starts with its own initial conditions. Figure 12 shows temperature difference versus precipitation difference (6–0.2 k) for 7 PMIP GCMs, ECHO-G and RCA3. The differences are calculated for two large regions that are resolved at the scale of the GCMs, northern Europe (5–50° E, 55–70° N) and southern Europe (10° W–50° E, 35–55° N) (blue boxes in Fig. 1). All model results share common features, but show some differences; the spread between models is largest in summer precipitation and winter temperature in northern Europe, and smallest in winter precipitation in southern Europe.

RCA3 follows ECHO-G to some extent, with the exception of summer precipitation in northern Europe. The land–sea distribution in the RCA3 simulations differs between 6 and 0.2 k (Fig. 1) with some grid boxes being sea at 6 k and land at 0.2 k. This difference leads to more convective precipitation at 0.2 k than at 6 k for these coastal regions (cf. Fig. 9). A similar effect is seen along the coast of the Mediterranean Sea. In ECHO-G the land–sea distribution is constant through time. Thus, for some coastal areas, the precipitation difference between 6 and 0.2 k is negative in the RCA3 simulation and positive in the ECHO-G simulation.

The choice of another GCM would obviously provide different results, but the difference is difficult to quantify. It is not obvious that the choice of another GCM would lead to generally larger or smaller temperature and precipitation differences. Furthermore, RCA3 partly produces its "own" climate. Interestingly enough, all of the GCMs show positive summer temperature differences between 6 and 0.2 k. It indicates that the temperature differences are positive in the model simulations as a result of the higher summer insolation at 6 k than at 0.2 k. For northern Europe, the pollen-based palaeoclimate reconstructions discussed above as well as all quantitative and qualitative temperature reconstructions based on other palaeoecological records than pollen indicate warmer conditions at 6k than at 0.2 k, in agreement with the GCMs. For southern Europe, climate model simulations and pollen-based reconstructions display different signs of the difference. The difference in signal between the GCMs (and RCA3) and the palaeoclimate reconstruction indicates either an alternative forcing offsetting the insolation differences or the influence of natural variability caused by circulation changes, which would yield a negative temperature difference between 6 and 0.2 k in southern Europe, i.e. lower temperatures at 6 k than at 0.2 k.

4.3 Comparison with other studies of land cover – climate interactions

For past climate, studies conducted with global models at a coarse spatial resolution show that the albedo effect

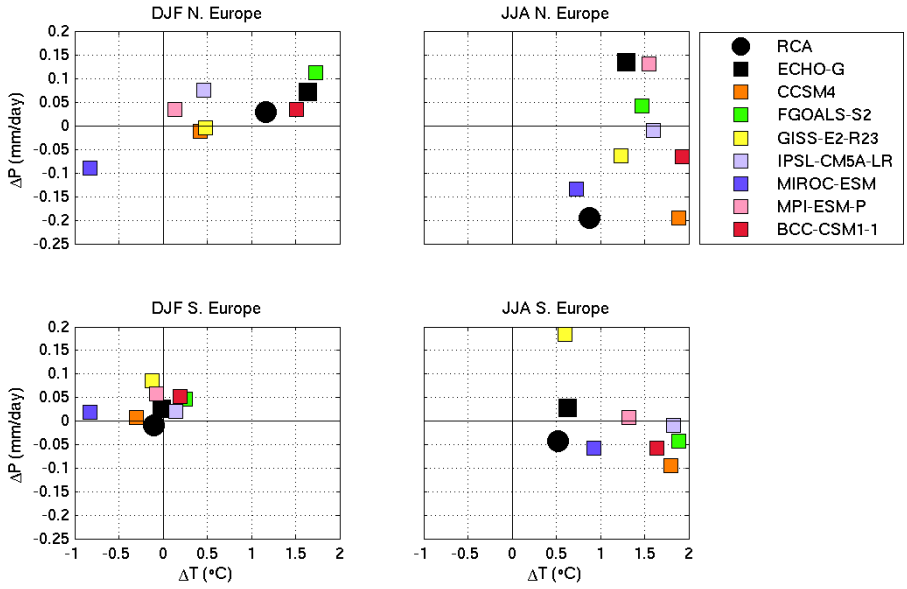

Fig. 12. Difference in temperature (ΔT) and precipitation (ΔP) between 6 and 0.2 k BP in winter (left) and summer (right) in northern Europe (top) and southern Europe (bottom). The results from GCMs are shown as coloured squares, and the result from the regional climate model RCA3 as a circle.

dominates over the other biogeophysical effects leading to a colder climate when deforestation increases in the Northern Hemisphere (e.g. Jahn et al., 2005; Brovkin et al., 2006; Pitman et al., 2009; Pongratz et al., 2009a; Goosse et al., 2012, He et al., 2014). Other experimental climate model studies with simulated deforestation in large parts of the globe show a similar effect on global mean temperature (Kleidon et al., 2000). Some studies have also shown regional differences in the effects of deforestation on climate, but the results from changing heat fluxes are described as ambiguous (Pitman et al., 2009) or hard to evaluate (Goosse et al., 2012).

Our results show that the albedo effect is indeed a major process in the vegetation–climate interactions, and they also provide a more detailed understanding of the relative importance of different biogeophysical processes. We show that land-cover changes can have significant effects on the simulated climate and be a driver of climate change at the regional scale. The albedo effect dominates in winter, especially in regions with a relatively long snow season. In summer, the albedo effect dominates in some regions, while changes in latent heat fluxes are more important in other regions. The differences in the importance of the various biogeophysical processes depend on the land-cover descriptions used and local geographical characteristics.

5 Conclusions

This study demonstrates that past European anthropogenic land-cover changes prior to AD 1850 were large enough to influence the regional climate. The temperature response varied by $\pm 1\,^{\circ}\mathrm{C}$ in summer depending on local/regional characteristics that can only be captured by high-resolution climate models such as RCA3.

The differences in simulated climate depend mainly on changes in the albedo and latent heat flux due to changes in vegetation cover. Which of the biogeophysical processes will be dominant depends on local/regional climate and vegetation characteristics. The results show that the effect of albedo dominates in winter, but that latent heat flux also plays an important role with regard to the differences in simulated climate in summer. Therefore, a comprehensive model including these effects is required in order to study effects of changing land cover on climate. At 6 k the differences between the land-cover descriptions (V, V + H3.1 or V + KK10) are small, leading to little difference between the simulated climates. At 0.2 k the differences between the land-cover descriptions are large enough to result in significantly different simulated climates. Depending on the estimate of deforestation, the difference between simulations varies in some regions between -1 and $0\,^{\circ}\mathrm{C}$ in seasonal mean winter temperature, -1 and $1\,^{\circ}\mathrm{C}$ in summer temperature and -30 and $0\,\mathrm{mm\,month^{-1}}$ in summer precipitation.

Even though the difference in climate is significant between simulations using different land-cover descriptions (V, V + H3.1 or V + KK10), it is not possible to assess which land-cover description is the most reasonable on the basis of a comparison of modelled climate with palaeoclimate reconstructions. This is because the uncertainties of the palaeoclimate reconstructions and the differences between them are at least as large as the differences between the climate simulations at both 6 and 0.2 k. Nevertheless, it is clear that

vegetation cover plays an important role in the regional climate and that a dynamic vegetation description is essential in regional climate modelling. The present study demonstrates that reliable reconstructions of past vegetation are necessary for a better understanding of past land cover–climate relationships in order to assess the role of changes in land cover in present and future climate change. Therefore, future research should include both evaluation of ALCC scenarios and the potential natural vegetation simulated by vegetation models using, for example, pollen-based methods such as the REVEALS reconstruction for NW Europe (Kaplan et al., 2014; Marquer et al., 2014).

In future modelling efforts, it will also be important to study the indirect effects from increasing atmospheric CO_2 (He et al., 2014), and a model-ensembles approach would be useful. This study shows that the choice of another GCM would provide overall similar results, but multiple simulations may help to distinguish the climate change signal from natural variability and to better quantify uncertainties.

Acknowledgements. All model simulations with the RCM were performed on the Swedish climate computing resources Gimle and Vagn funded with a grant from the Knut and Alice Wallenberg foundation. Qiong Zhang helped collecting PMIP data. This study is a part of the LANDCLIM (LAND cover–CLIMate interactions in NW Europe during the Holocene) project and research network coordinated by M.-J. Gaillard and sponsored by the Swedish Research Council [VR], the Nordic Council of Ministers [NordForsk] and MERGE (see below). It is also a contribution to the Swedish strategic research areas ModElling the Regional and Global Earth system (MERGE) and Biodiversity and Ecosystem Services in a Changing Climate (BECC).

Edited by: V. Rath

References

Bala, G., Caldeira, K., Wickett, M., Phillips, T. J., Lobell, D. B., Delire, C., and Mirin, A.: Combined climate and carbon-cycle effects of large-scale deforestation, Proc. Natl. Acad. Sci., 104, 6550–6555, doi:10.1073/pnas.0608998104, 2007.

Ban-Weiss, G. A., Bala, G., Cao, L., Pongratz, J., and Caldeira, K.: Climate forcing and response to idealized changes in surface latent and sensible heat, Environ. Res. Lett., 6, 034032, doi:10.1088/1748-9326/6/3/034032, 2011.

Bartlein, P. J., Harrison, S. P., Brewer, S., Connor, S., Davis, B. A. S., Gajewski, K., Guiot, J., Harrison-Prentice, T. I., Henderson, A., Peyron, O., Prentice, I. C., Scholze, M., Seppä, H., Shuman, B., Sugita, S., Thompson, R. S., Viau, A. E., Williams, J., and Wu, H.: Pollen-based continental climate reconstructions at 6 and 21 ka: a global synthesis, Clim. Dynam., 37, 775–802, 2010.

Berger, A. and Loutre, M. F.: Insolation values for the climate of the last 10 million years, Quaternary Sci. Rev., 10, 29–317, 1991.

Bigler, C., Grahn, E., Larocque, I., Jeziorski, A., and Hall, R.: Holocene environmental change at Lake Njulla (999 m a.s.l.), northern Sweden: a comparison with four small nearby lakes along an altitudinal gradient, J. Paleolimnol., 29, 13–29, 2003.

Bigler, C., Barnekow, L., Heinrichs, M. L., and Hall, R. I.: Holocene environmental history of Lake Vuolop Njakajaure (Abisko National Park, northern Sweden) reconstructed using biological proxy indicators, Veget. Hist. Archaebot., 15, 309–320, 2006.

Bond, G., Kromer, B., Beer, J., Muscheler, R., Evans, M. N., Showers, W., Hoffmann, S., Lotti-Bond, R., Hajdas, I., and Bonani, G.: Persistent solar influence on North Atlantic climate during the Holocene, Science, 294, 2130–2136, 2001.

Borgmark, A.: Holocene climate variability and periodicities in south-central Sweden interpreted from peat humification analysis, Holocene, 15, 387–395, 2005.

Boyle, J. F., Gaillard, M.-J., Kaplan, J. O., and Dearing, J. A.: Modelling prehistoric land use and carbon budgets: A critical review, Holocene, 21, 715–722, 2011.

Brovkin, V., Claussen, M., Driesschaert, E., Fichefet, T., Kicklighter, D., Loutre, M. F., Matthews, H. D., Ramankutty, N., Schaeffer, M., and Sokolov, A.: Biogeophysical effects of historical land cover changes simulated by six Earth system models of intermediate complexity, Clim. Dynam., 26, 587–600, doi:10.1007/s00382-005-0092-6, 2006.

Christidis, N., Stott, P. A., Hegerl, G. C., and Betts, R. A.: The role of land use change in the recent warming of daily extreme temperatures, Geophys. Res. Lett., 40, 589–594, doi:10.1002/grl.50159, 2013.

Davis, B. A. S., Brewer, S., Stevenson, A. C., and Guiot, J.: The temperature of Europe during the Holocene reconstructed from pollen data, Quaternary Sci. Rev., 22, 1701–1716, 2003.

Davis, B. A. S., Zanon, M., Collins, P., Mauri, A., Bakker, J., Barboni, D., Barthelmes, A., Beaudouin, C., Bjune, A. E., Bozilova, E., Bradshaw, R. H. W., Brayshay, B. A., Brewer, S., Brugiapaglia, E., Bunting, J., Connor, S. E., Beaulieu, J.-L., Edwards, K., Ejarque, A., Fall, P., Florenzano, A., Fyfe, R., Galop, D., Giardini, M., Giesecke, T., Grant, M. J., Guiot, J., Jahns, S., Jankovská, V., Juggins, S., Kahrmann, M., Karpińska-Kołaczek, M., Kołaczek, P., Kühl, N., Kuneš, P., Lapteva, E. G., Leroy, S. A. G., Leydet, M., López Sáez, J. A., Masi, A., Matthias, I., Mazier, F., Meltsov, V., Mercuri, A. M., Miras, Y., Mitchell, F. J. G., Morris, J. L., Naughton, F., Nielsen, A. B., Novenko, E., Odgaard, B., Ortu, E., Overballe-Petersen, M. V., Pardoe, H. S., Peglar, S. M., Pidek, I. A., Sadori, L., Seppä, H., Severova, E., Shaw, H., Święta-Musznicka, J., Theuerkauf, M., Tonkov, S., Veski, S., Knaap, W. O., Leeuwen, J. F. N., Woodbridge, J., Zimny, M., and Kaplan, J. O.: The European Modern Pollen Database (EMPD) project, Veget. Hist. Archaeobot., 22, 521–530, doi:10.1007/s00334-012-0388-5, 2013.

De Noblet-Ducoudré, N., Boisier, J.-P., Pitman, A., Bonan, G. B., Brovkin, V., Cruz, F., Delire, C., Gayler, V., van den Hurk, B. J. J. M., Lawrence, P. J., van der Molen, M. K., Müller, C., Reick, C. H., Strengers, B. J., and Voldoire, A.: Determining Robust Impacts of Land-Use-Induced Land Cover Changes on Surface Climate over North America and Eurasia: Results from the First Set of LUCID Experiments, J. Climate, 25, 3261–3281, doi:10.1175/JCLI-D-11-00338.1, 2012

Deser, C., Knutti, R., Solomon, S., and Phillips A. S.: Communication of the role of natural variability in future North American climate, Nat. Clim. Change, 2, 775–779, doi:10.1038/nclimate1562, 2012.

Digerfeldt, G.: Reconstruction and regional correlation of Holocene lake-level fluctuations in Lake Bysjön, South Sweden, Boreas, 17, 165–182, 1998.

Efron, B.: Bootstrap methods: Another look at the jackknife, Ann. Statist., 7, 1–26, 1979.

Flückiger, J., Monnin, E., Stauffer, B., Schwander, J., Stocker, T., Chappellaz, J., Raynaud, D., and Barnola, J. M.: High resolution Holocene N_2O ice core record and its relationship with CH_4 and CO_2, Global Biogeochem. Cy., 16, 10-1–10-8, doi:10.1029/2001GB001417, 2002.

Forster, P., Ramaswamy, V., Artaxo, P., Berntsen, T., Betts, R., Fahey, D. W., Haywood, J., Lean, J., Lowe, D. C., Myhre, G., Nganga, J., Prinn, R., Raga, G., Schulz, M., and Van Dorland, R.: Radiative forcing of climate change, in: Climate Change 2007: The Physical Science Basis. Contribution of Working Group I to the Fourth Assessment Report of the Intergovernmental Panel on Climate Change, edited by: Solomon, S., Qin, D., Manning, M., Chen, Z., Marquis, M., Averyt, K. B., Tignor, M., and Miller, H. L., Cambridge and New York, NY, Cambridge University Press, 129–234, 2007.

Gaillard, M.-J.: Archaeological Applications, in: The Encyclopedia of Quaternary Science 3, edited by: Elias S. A., Elsevier, Amsterdam, 880–904, 2013.

Gaillard, M.-J., Sugita, S., Mazier, F., Trondman, A.-K., Broström, A., Hickler, T., Kaplan, J. O., Kjellström, E., Kokfelt, U., Kuneš, P., Lemmen, C., Miller, P., Olofsson, J., Poska, A., Rundgren, M., Smith, B., Strandberg, G., Fyfe, R., Nielsen, A. B., Alenius, T., Balakauskas, L., Barnekow, L., Birks, H. J. B., Bjune, A., Björkman, L., Giesecke, T., Hjelle, K., Kalnina, L., Kangur, M., van der Knaap, W. O., Koff, T., Lagerås, P., Latałowa, M., Leydet, M., Lechterbeck, J., Lindbladh, M., Odgaard, B., Peglar, S., Segerström, U., von Stedingk, H., and Seppä, H.: Holocene land cover reconstructions for studies on land cover-climate feedbacks, Clim. Past, 6, 483–499, doi:10.5194/cp-6-483-2010, 2010.

Giorgi, F. and Mearns, L. O.: Introduction to special section: Regional climate modelling revisited, J. Geophys. Res., 104, 6335–6352, 1999.

Gómez-Navarro, J. J., Montávez, J. P., Jerez, S., Jiménez-Guerrero, P., Lorente-Plazas, R., González-Rouco, J. F., and Zorita, E.: A regional climate simulation over the Iberian Peninsula for the last millennium, Clim. Past, 7, 451–472, doi:10.5194/cp-7-451-2011, 2011.

Gómez-Navarro, J. J., Montávez, J. P., Jiménez-Guerrero, P., Jerez, S., Lorente-Plazas, R., González-Rouco, J. F., and Zorita, E.: Internal and external variability in regional simulations of the Iberian Peninsula climate over the last millennium, Clim. Past, 8, 25–36, doi:10.5194/cp-8-25-2012, 2012.

Goosse, H., Guiot, J., Mann, M. E., Dubinkina, S., and Sallaz.Damaz, Y.: The medieval climate anomaly in Europe: Comparison of the summer and annual mean signals in two reconstructions and in simulations with data assimilation, Global Planet. Change, 84–85, 35–47, 2012.

Graham, L. P., Olsson, J., Kjellström, E., Rosberg, J., Hellström, S.-S., and Berndtsson, R.: Simulating river flow to the Baltic Sea from climate simulations over the past millennium, Boreal Environ. Res., 14, 173–182, 2009.

Grudd, H.: A 7400-year tree-ring chronology in northern Swedish Lapland: natural climatic variability expressed on annual to millenial timescales, Holocene, 12, 657–665, 2002.

Hammarlund, D., Björck, S., Buchardt, B., Israelson, C., and Thomsen, C. T.: Rapid hydrological changes during the Holocene revealed by stable isotope records of lacustrine carbonates from Lake Igelsjön, southern Sweden, Quaternary Sci. Rev., 22, 353–370, 2003.

Hammarlund, D., Velle, G., Wolfe, B. B., Edwards, T. W. D., Barnekow, L., Bergman, J., Holmgren, S., Lamme, S., Snowball, I., Wohlfarth, B., and Possnert, G.: Palaeolimnological responses to Holocene forest retreat in the Scandes Mountains, west-central Sweden, Holocene, 14, 862–876, 2004.

Harrison, S. P., Jolly, D., Laarif, F., Abe-Ouchi, A., Dong, B., Herterich, K., Hewitt, C., Joussaume, S., Kutzbach, J. E., Mitchell, J., de Noblet, N., and Valdes, P.: Intercomparison of Simulated Global Vegetation Distributions in Response to 6 kyr BP Orbital Forcing, J. Climate, 11, 2721–2742, 1998.

He, F., Vavrus, S. J., Kutzbach, J. E., Ruddiman, W. F., Kaplan, J. O., and Krumhardt, K. M.: Simulating global and local surface temperature changes due to Holocene anthropogenic land cover change, Geophys. Res. Lett., 41, 623–631, doi:10.1002/2013GL058085, 2014.

Helama, S., Lindholm, M., Timonen, M., Meriläinen, J., and Eronen, M.: The supra-long Scots pine tree-ring record for Finnish Lapland. Part 2: Interannual to centennial variability in summer temperatures for 7500 years, The Holocene, 12, 681–687, 2002.

Hickler, T., Smith, B., Sykes, M. T., Davis, M. B., Sugita, S. and Walker, K.: Using a generalized vegetation model to simulate vegetation dynamics in northeastern USA, Ecology, 85, 519–530, 2004.

Hickler, T., Vohland, K., Feehan, J., Miller, P. A., Smith, B., Costa, L., Giesecke, T., Fronzek, S., Carter, T. R., Cramer, W., Kühn, I., and Sykes, M. T.: Projecting the future distribution of European potential natural vegetation zones with a generalized, tree species-based dynamic vegetation model, Global Ecol. Biogeogr., 21, 50–63, 2012.

Hughes, P. D. M., Barber, K. E., Langdon, P. G., and Mauquoy, D.: Mire-development pathways and palaeoclimatic records from a full Holocene peat archive at Walton Moss, Cumbria, England, Holocene, 10, 465–479, 2000.

HYDE: available at: http://themasites.pbl.nl/en/themasites/hyde/download/index.html (last access: 13 December 2011), 2011.

Ikonen, L.: Holocene development and peat growth of the raised bog Pesänsuo in southwestern Finland, Bulletin, Vol. 370, Geological Survey of Finland, Espoo, 1993.

Jahn, A., Claussen, M., Ganopolski, A., and Brovkin, V.: Quantifying the effect of vegetation dynamics on the climate of the Last Glacial Maximum, Clim. Past, 1, 1–7, doi:10.5194/cp-1-1-2005, 2005.

Kaplan, J., Krumhardt, K., and Zimmermann, N.: The prehistoric and preindustrial deforestation of Europe, Quaternary Sci. Rev., 28, 3016–3034, 2009.

Kaplan, J. O., Krumhardt, K. M., Ellis, E. C., Ruddiman, W. F., Lemmen, C. and Goldewijk, K. K.: Holocene carbon emissions as a result of anthropogenic land cover change, The Holocene, 21, 775–791, doi:10.1177/0959683610386983, 2011.

Kaplan, J. O., Krumhardt, K. M., Gaillard, M.-J., Sugita, S., Trondman, A.-K., and Mazier, F.: The deforestation history of

northwest Europe: Evaluating anthropogenic land cover change scenarios with pollen-based landscape reconstructions, in preparation, 2014.

Kaspar, F., Spangehl, T., and Cubasch, U.: Northern hemisphere winter storm tracks of the Eemian interglacial and the last glacial inception, Clim. Past, 3, 181–192, doi:10.5194/cp-3-5 181-2007, 2007.

Kjellström, E., Brandefelt, J., Näslund, J. O., Smith, B., Strandberg, G., Voelker, A. H. L., and Wohlfarth, B.: Simulated climate conditions in Fennoscandia during a MIS 3 stadial, Boreas, 10, 436–456, doi:10.1111/j.1502-3885.2010.00143.x, 2010

Kjellström, E., Nikulin, G., Hansson, U., Strandberg, G., and Ullerstig, A.: 21st century changes in the European climate: uncertainties derived from an ensemble of regional climate model simulations, Tellus A, 63, 24–40, 2011.

Kleidon, A., Fraedrich, K., and Heimann, M.: A green planet versus a desert world: Estimating the maximum effect of vegetation on the land surface climate, Clim. Change, 44, 471–493, 2000.

Klein Goldewijk, K., Beusen, A., de Vos, M., and van Drecht, G.: The HYDE 3.1 spatially explicit database of human induced land use change over the past 12,000 years, Global Ecol. Biogeogr., 20, 73–86, 2011.

Kohfeld, K. E. and Harrison, S. P.: How well can we simulate past climates? Evaluating the models using global palaeoenvironmental datasets, Quaternary Sci. Rev., 19, 321–346, 2000.

Korhola, A., Weckström, J., Holmström, L., and Erästö, P.: A quantitative Holocene climatic record from diatoms in northern Fennoscandia, Quaternary Res., 54, 284–294, 2000.

Laroque, I. and Hall, R. I.: Holocene temperature estimates and chironomid community composition in the Abisko valley, northern Sweden, Quaternary Sci. Rev., 23, 2453–2465, 2004.

Legutke, S. and Voss, R.: The Hamburg atmosphere-ocean coupled circulation model ECHOG, DKRZ-Report, German Climate Computer Centre (DKRZ), Hamburg, Germany, 1999.

Magny, M.: Holocene climate variability as reflected by mid-European lake-level fluctuations and its probable impact on prehistoric human settlements, Quaternary Int., 113, 65–79, 2004.

Magny, M.: Holocene fluctuations of lake levels in west-central Europe: methods of reconstruction, regional pattern, palaeoclimatic significance and forcing factors, Encyclopedia of Quaternary Science, edited by: Elias, S., Elsevier, Oxford, 1389–1399, 2007.

Magny, M. and Combourieu Nebout, N.: Holocene changes in environment and climate in the central Mediterranean as reflected by lake and marine records, Clim. Past, 9, 1447–1454, doi:10.5194/cp-9-1447-2013, 2013.

Magny, M., Combourieu+Nebout, N., de Beaulieu, J. L., Bout-Roumazeilles, V., Colombaroli, D., Desprat, S., Francke, A., Joannin, S., Ortu, E., Peyron, O., Revel, M., Sadori, L., Siani, G., Sicre, M. A., Samartin, S., Simonneau, A., Tinner, W., Vannière, B., Wagner, B., Zanchetta, G., Anselmetti, F., Brugiapaglia, E., Chapron, E., Debret, M., Desmet, M., Didier, J., Essallami, L., Galop, D., Gilli, A., Haas, J. N., Kallel, N., Millet, L., Stock, A., Turon, J. L., and Wirth, S.: North-south palaeohydrological contrasts in the central Mediterranean during the Holocene: tentative synthesis and working hypotheses, Clim. Past, 9, 2043–2071, doi:10.5194/cp-9-2043-2013, 2013.

Marquer, L., Gaillard, M.-J., Sugita, S., Poska, A., Trondman, A.-K., Mazier, F., Nielsen, A. B., Fyfe, R. M., Kaplan, J. O., Vad Odgaard, B., Smith, B., Alenius, T., Birks, H. J. B., Bjune, A. E., Christiansen, J., Dodson, J., Edwards, K. J., Giesecke, T., Herzschuh, U., Kangur, M., Koff, T., Latałowa, M., Lechterbeck, J., Lorenz, S., Schultr, M., and Seppä, H.: Climate and human-induced changes in Holocene plant diversity and ecology in western/central and northern Europe: new insights based on land-cover reconstruction and modelling, in preparation, 2014.

Masson, V., Cheddadi, R., Braconnot, P., Joussaume, S., Texier, D., and PMIP participants: Mid-Holocene climate in Europe: what can we infer from PMIP model-data comparisons?, Clim. Dynam., 15, 163–182, 1999.

Mauri, A., Davis, B. A. S., Collins, P. M., and Kaplan, J. O.: The influence of atmospheric circulation on the mid-Holocene climate of Europe: a data-model comparison, Clim. Past Discuss., 9, 5569–5592, doi:10.5194/cpd-9-5569-2013, 2013.

Nielsen, A. B., Kokfelt, U., Rundgren, M., and Gaillard, M.-J.: A review of proxy based climate reconstructions for Northwest Europe in the time slices 6000 BP and 200 BP, in preparation, 2014.

Niggeman, S., Mangini, A., Richter, D. K., and Wurth, G.: A paleoclimate record of the last 17.600 years from the B7 cave, Sauerland, Germany, Quaternary Sci. Rev., 22, 555–567, 2003.

Nikulin, G., Kjellström, E., Hansson, U., Strandberg, G., and Ullerstig, A.: Evaluation and future projections of temperature, precipitation and wind extremes over Europe in an ensemble of regional climate simulations, Tellus A, 63, 41–55, 2011.

Olofsson, J.: The Earth – climate and anthropogenic interactions in a long time perspective, PhD-thesis, Dept of Physical Geography and Ecosystem Science, Lund, 2013.

Olofsson, J. and Hickler, T.: Effects of human land-use on the global carbon cycle during the last 6,000 years, Veget. Hist. Archaeobot., 17, 606–615, 2008.

Olsen, J., Noe-Nygaard, N., and Wolfe, B. B.: Mid to Late Holocene climate variability and anthropogenic impacts; multi-proxy evidence from lake Bliden, Denmark, J. Paleolimnol., 43, 323–343, 2010.

Pausas, J. G.: Changes in fire and climate in the eastern Iberian Peninsula (Mediterranean basin), Clim. Change, 63, 337–350, 2004.

Peltier, W. R.: Global glacial isostasy and the surface of the ice-age circulation. Earth: The ICE-5G (VM2) model and GRACE, Ann. Rev. Earth Planet. Sci., 32, 111–149, 2004.

Peyron, O., Guiot, J., Cheddadi, R., Tarasov, P., Reille, M., de Beaulieu, J.-L., Bottema, S., and Andrieu, V.: Climatic Reconstruction in Europe for 18,000 YR B.P. from Pollen Data, Quaternary Res., 49, 183–196, 1998.

Peyron, O., Magny, M., Goring, S., Joannin, S., de Beaulieu, J.-L., Brugiapaglia, E., Sadori, L., Garfi, G., Kouli, K., Ioakim, C., and Combourieu-Nebout, N.: Contrasting patterns of climatic changes during the Holocene across the Italian Peninsula reconstructed from pollen data, Clim. Past, 9, 1233–1252, doi:10.5194/cp-9-1233-2013, 2013.

Pielke Sr., R. A., Pitman, A., Niyogi, D., Mahmood, R., McAlpine, C., Hossain, F., Klein Goldewijk, K., Nair, U., Betts, R., Fall, S., Reichstein, M., Kabat, P., and de Noblet, N.: Land use/land cover changes and climate: modeling analysis and observational evidence, WIREs Clim. Change, 2, 828–850, doi:10.1002/wcc.144, 2011.

Pitman, A. J., de Noblet-Ducoudre, N., Cruz, F. T., Davin, E. L., Bonan, G. B., Brovkin, V. Claussen, M., Delire, C., Ganzeveld,

L., Gayler, V., van den Hurk, B. J. J. M., Lawrence, P. J., van der Molen, M. K., Muller, C., Reick, C. H., Seneviratne, S. I., Strengers, B. J., and Voldoire, A.: Uncertainties in climate responses to past land cover change: First results from the LUCID intercomparison study, Geophys. Res. Lett., 36, L14814, doi:10.1029/2009GL039076, 2009.

Pongratz, J., Raddatz, T., Reick, C. H., Esch, M., and Claussen, M.: Radiative forcing from anthropogenic land cover change since A.D. 800, Geophys. Res. Lett., 36, L02709, doi:10.1029/2008GL036394, 2009a.

Pongratz, J., Reick, C. H., Raddatz, T., and Claussen, M.: Effects of anthropogenic land cover change on the carbon cycle of the last millennium, Global Biogeochem. Cy., 23, GB4001, doi:10.1029/2009GB003488, 2009b.

Pongratz, J., Reick, C. H., Raddatz, T., and Claussen, M.: Biogeophysical versus biogeochemical climate response to historical anthropogenic land cover change, Geophys. Res. Lett., 37, L08702, doi:10.1029/2010GL043010, 2010.

Prentice, I. C., Guiot, J., Huntley, B., Jolly, D., and Cheddadi, R.: Reconstructing biomes from palaeoecological data: a general method and its application to European pollen data at 0 and 6 ka, Clim. Dynam., 12, 185–194, 1996.

Räisänen, J., Hansson, U., Ullerstig, A., Döscher, R., Graham, L. P., Jones, C., Meier, H. E. M., Samuelsson, P., and Willén, U: European climate in the late twenty-first century: regional simulations with two driving global models and two forcing scenarios, Clim. Dynam., 22, 13–31, 2004.

Rosén, P., Segerström, U., Eriksson, L., Renberg, I., and Birks, H. J. B.: Holocene climatic change reconstructed from diatoms, chironomids, pollen and near-infrared spectroscopy at an alpine lake (Sjuodjijaure) in northern Sweden, Holocene, 11, 551–562, 2001.

Ruddiman, W. F.: The anthropogenic greenhouse era began thousands of years ago, Clim. Change, 61, 261–293, 2003.

Rummukainen, M.: State-of-the-art with regional climate models, WIREs Clim. Change, 1, 82–96, doi:10.1002/wcc.8, 2010

Rummukainen, M., Räisänen, J., Bringfelt, B., Ullerstig, A., Omstedt, A., Willén, U., Hansson, U., Jones, C., and Jones, C.: A regional climate model for northern Europe: model description and results from the downscaling of two GCM control simulations, Clim. Dynam., 17, 339–359, 2001.

Samuelsson, P., Jones, C. G., Willen, U., Ullerstig, A., Gollvik, S., Hansson, U., Jansson, C., Kjellström, E., Nikulin, G., and Wyser, K.: The Rossby Centre regional climate model RCA3: model description and performance, Tellus A, 63, 4–23, doi:10.1111/j.1600-0870.2010.00478.x, 2011.

Schimanke, S., Meier, H. E. M., Kjellström, E., Strandberg, G., and Hordoir, R.: The climate in the Baltic Sea region during the last millennium simulated with a regional climate model, Clim. Past, 8, 1419–1433, doi:10.5194/cp-8-1419-2012, 2012.

Sitch, S., Smith, B., Prentice, I.C., Arneth, A., Bondeau, A., Cramer, W., Kaplan, J. O., Levis, S., Lucht, W., Sykes, M. T., Thonicke, K., and Venevsky, S.: Evaluation of ecosystem dynamics, plant geography and terrestrial carbon cycling in the LPJ dynamic global vegetation model, Global Change Biol., 9, 161–185, 2003.

Smith, B., Prentice, I. C., and Sykes, M. T.: Representation of vegetation dynamics in modelling of terrestrial ecosystems: comparing two contrasting approaches within European climate space, Global Ecol. Biogeogr., 10, 621–637, 2001.

Snowball, I. and Sandgren, P.: Lake sediment studies of Holocene glacial activity, northern Sweden: contrasts in interpretation, Holocene, 6, 367–372, 1996.

Solanki, S. K., Usoskin, I. G., Kromer, B., Schussler, M., and Beer, J.: Unusual activity of the Sun during recent decades compared to the previous 11,000 years, Nature, 431, 1084–1087, 2004.

Spracklen, D. V., Arnold, S. R., and Taylor, C. M.: Observations of increased tropical rainfall preceded by air passage over forests, Nature, 489, 282–286, doi:10.1038/nature11390, 2012.

Strandberg, G., Brandefelt, J., Kjellström, E., and Smith, B.: High-resolution regional simulation of the last glacial maximum climate in Europe, Tellus A, 63, 107–125, 2011.

Sugita, S.: Theory of quantitative reconstruction of vegetation I: pollen from large sites REVEALS regional vegetation composition, Holocene, 17, 229–241, 2007.

Trondman, A.-K., Gaillard, M.-J., Sugita, S., Mazier, F., Fyfe, R., Lechterbeck, J., Marquer, L., Nielsen, A.B., Twiddle, C., Barratt, P., Birks, H.J.B., Bjune, A.E., Caseldine, C., David, R., Dodson, J., Dörfler, W., Fischer, E., Giesecke, T., Hultberg, T., Kangur, M., Kuneš, P., Latalowa, M., Leydet, M., Lindbaldh, M., Mitchell, F., Odgaard, B., Peglar, S.M., Persson, T., Rösch, M., van der Knaap, P., van Geel, B., Smith, A., and Wick, L.: Pollen-based land-cover reconstructions for the study of past vegetation-climate interactions in NW Europe at 0.2k, 0.5k, 3k and 6k years before present, J. Global Biol., submitted, 2013.

Vannière, B., Power, M. J., Roberts, N., Tinner, W., Carrién, J., Magny, M., Bartlein, P., Colombaroli, D., Daniau, A.-L., Finsinger, W., Gil-Romera, G., Kaltenrieder, P., Magri, D., Pini, R., Sadori, L., Turner, R., Valsecchi, V., and Vescovi, E.: Circum-Mediterranean fire activity and climate changes during the mid-Holocene environmental transition (8500–2500 cal.BP), The Holocene, 21, 53–73, doi:10.1177/0959683610384164, 2011.

Velle, G., Brooks, S. J., Birks, H. J. B., and Willassen, E.: Chironomids as a tool for inferring Holocene climate: an assessment based on six sites in southern Scandinavia, Quaternary Sci. Rev., 24, 1429–1462, 2005.

Vork, K. A. and Thomsen E.: Lusitanian/Mediterranean ostracods in the Holocene of Denmark: implications for the interpretation of winter temperatures during the postglacial temperature maximum, Holocene, 6, 423–432, 1996.

Wagner, S., Widmann, M., Jones, J., Haberzettl, T., Lücke, A., Mayr, C., Ohlendorf, C., Schäbitz, F., and Zolitschka, B.: Transient simulations, empirical reconstructions and forcing mechanism for the Mid-holocene hydrological climate in Southern Patagonia, Clim. Dynam., 29, 333–355, 2007.

Wolf, A., Callaghan, T. V., and Larson, K: Future changes in vegetation and ecosystem function of the Barents Region, Clim. Change, 87, 51–73, 2008.

Wramneby, A., Smith, B., and Samuelsson, P.: Hot spots of vegetation-climate feedbacks under future greenhouse forcing in Europe, J. Geophys. Res., 115, D21119, doi:10.1029/2010JD014307, 2010.

Zorita, E., Gonzalez-Rouco, J. F., von Storch, H., Montavez, J. P., and Valero, F.: Natural and anthropogenic modes of surface temperature variations in the last thousand years, Geophys. Res. Lett., 32, L08707, doi:10.1029/2004GL021563, 2005.